Reaction Mechanisms and Environments of Active Sites of Hydrogenations on Metal Catalysts

（金属触媒上の水素化反応機構と活性点の反応環境に関する研究）

Hideaki Yoshitake

吉武英昭

(1)

Reaction Mechanisms and Environments of Active Sites of Hydrogenations on Metal Catalysts

by

Hideaki Yoshitake

A Thesis Submitted to The University of Tokyo
in Fulfillment of the Requirements for
The Degree of Doctor of Science

January, 1992

Acknowledgements

I would like to express my gratitude to Professor Yasuhiro Iwasawa for his continuous academic guidance and encouragement. The works described in this thesis have been carried out under his supervision.

I am grateful to Dr. Kiyotaka Asakura for his valuable advice. I am also grateful to the staffs of KEK-PF (Photon Factory of National Laboratory for High Energy Physics) for X-ray absorption measurements and Professor Takaharu Onishi, Professor Kazunari Domen and Dr. Akihiko Kudo for using X-ray photoemission spectroscopic apparatus.

Discussion at the colloquium of Prof. Iwasawa's laboratory was useful for better understanding of the experimental data and general knowledge of physical chemistry. I express hearty thank to all the people of the laboratory. Finally, I thank Professor Ken-ichiro Ota for his kind suggestion and help in writing this thesis.

Content

Chapter 1

General Introduction

1.1 Heterogeneity of Catalyst Surface and Chemical Reactions

Chemical reactions occurring on a solid surface are under control of the heterogeneity of the surface. One of the typical and most important cases of them is heterogeneous catalysis. This idea has appeared everywhere in the history of the study on catalysis. Most of all pioneering workers in their days were concerned with what the site for adsorption, reaction or desorption was and how the processes among them was. [1] It is not too much to be said that the heterogeneity of surface has been always in the center of the field. It was natural in a sense to start at the reaction on the flat dense surface when the physicochemical techniques were developed enough to investigate the single crystal surface and the high quality vacuum was obtainable, because flat surface could offer a standard which had not appeared before them. Then sparse or stepped surface came up in the interest to exploit chemistry of the surface heterogeneity. These studies contributed to the elucidation of the kind of site which is active to the key step and the surface processes between sites. [2]

In general, the surface of metal, of fine particle or single crystal, has kinds of atoms which have their own environment. Cuboctahedral fine particle of Ru, for example, consists of atoms in edge, corner and plain. It was concluded that ethane hydrogenolysis;

$$CH_3\text{-}CH_3 + H_2 \rightarrow 2CH_4$$

was active on edge and corner atoms. [3] Fe(111) has two kinds of atoms accessible to N_2 under NH_3 synthesis condition. And the active site was proved to be C_7 atom (its coordination number is 7). [4] These conclusions were based on the reasonable key steps for the overall reactions, C-C disruption and N_2 dissociative

adsorption, respectively. These examples were structural chemistry well related with reactivity to prove questions arising from the concerns of the idea above. In this way, surface heterogeneity includes various possibilities of the reaction on it and chemistry unexpected from the conventional idea can be developed.

A problem which arises in the recent studies of the surface science is the surface mobility. That is, solid surface is very reactive and the structure is often modified by the gaseous or liquid reactants. This is serious especially in the discussion of heterogeneity because microscopic investigation is needed for a certain spatially restricted area whose mobility is often high. The stable and fixed atoms are also inactive to the gas phase reactants. This involves potential effects on the overall catalytic reaction such as the site or intermediate activation by gas molecule and adsorbate-adsorbate interaction through the intermediary of surface. Thus the study on the surface in a working state is essential to study of heterogeneity and, further, dynamics of microscopic surface is the key for the elucidate of the genesis and origin of catalysis.

Promotion in solid catalyst by support or additives has been one of the topics in science and technology of catalysis. [5-11] This is not intended to be an alchemy but brings about the control of the function --- selectivity, activity and life time of the catalyst. Ammonia synthesis catalyst, which is a milestone of the field, is famous of the double promotion by potassium-additive (believed as electron donar) and Al_2O_3-support (to extend life time). The structure of the original catalyst components would be changed more or less by the promotion accompanied with alternation of the electronic state. Influence

on the microstructure of the catalyst is larger and more serious than expected from the change of net catalysis. And recent development of physicochemical method can gradually make it clear. This kind of study itself--- determination of local structure or the state of the small particles and surfaces --- is charming and gathers many investigators engaged in these techniques. Their contribution might build the static picture of the catalyst particles and surfaces in detail which makes a background and a base for the reaction on them. One important aspect of promotion is that it is inevitably a cause of heterogeneity. There must be conjunctions of the different phases --- an additive to metal particles or a support to metal particles --- and the composing element is usually different between two phases so that the exploitation of chemical processes occurring on heterogeneous surface is easier. Promotion might bring about model catalyst for the heterogeneity. Moreover, it is likely that microscopic reaction processes on the promoted surface involves totally new principle of chemical reaction which can not emerge on the non-promoted metal surface. In this meaning, investigation of the microscopic reaction mechanism on the promoted catalyst may contribute considerably to chemistry of solid surface.

The typical and fundamental problem happens in the study of chemical reaction on promoted catalyst is that the conjunction of different components on the solid surface can effect on catalyses in two manners. One is mere a combination of the each function, which can reduce the number of industrial processes in the plant, such as Al_2O_3 supported Pt catalyst for petroleum reforming. It is believed that Pt dehydrates alkanes into alkenes, Al_2O_3 isomerizes alkenes into branched alkenes and finally Pt

hydrogenates branched alkenes into branched alkanes. In this mechanism, each function can generate by itself and the reactants and intermediates go through each reaction each phase owns. The other is cooperation of two phases in a microscopic level, such as the generation of intermediate at the boundary. The function can not be observed if two components are separated. In order to distinguish them and clarify the phenomena as molecular processes, reaction mechanism including the active sites and their environments must be elucidated. It is needless to say that the approach should not be apart from the reaction condition, i.e., the working state of the catalyst surface.

The literature deals with modes of interaction of gas molecule and catalyst surface which includes heterogeneity in its heart of the discussion. Consider carbon monoxide adsorbed on a supported metal catalyst for example. Several patterns of interaction can be listed;

1. S-M-CO like

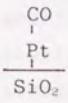

2. M-S-CO like

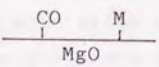

3. M — S like

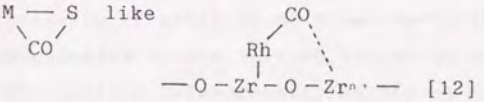

[12]

4. M-CO-S like

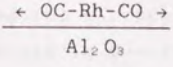

[13]

where M is a metal and S is a support. Every interaction of every pattern is different from the two body interaction but case 2 and sometimes case 1 may be considered as an two body problem. These systems are often trivial and should be only combination of the functions of the metal and the support in the reaction. 3. is an adsorbate generated in the boundary of the metal particle and the support. 4. is metal diffusion on the support induced by adsorbate. These are examples of the cooperative conjunction of metal particles and supports.

The orientation of the adsorbed molecule should be discussed when it has internal degree of freedom. This often determines regio- and stereo-selectivity in catalytic reaction. Combination of several methods, for example, infrared spectroscopy, electron spin resonance, extended X-ray absorption fine structure, is needed and/or defines more in the elucidation of these surface chemistry of dynamic processes.

The mode of interaction of each intermediate state is connected to the catalysis. Discussion above is the bases of the mechanisms of heterogeneous surface reaction. Conversion of each mode, constitution or population of intermediate states and interaction of each mode arise with problem of "time" to make the clarification of the phenomena difficult. It is true that the elucidation of an activation mode of a reactant which determines selectivity or activity of given catalyst is important. But the comprehensive vision of time evolution of the modes in relation to the surface heterogeneity should be necessary to the precise design of catalysts in future.

This thesis aims the elucidation of the chemical processes and mode of interactions in the intermediate state occurring on

the heterogeneous surface by several probe reactions. It is one of the effective approaches to the genesis of the heterogeneous catalysis. The systems chosen were hydrogenation of unsaturated compounds on noble metals supported on transition metal oxides and alkali metal-promoted Pt/SiO_2 which were investigated by kinetics, isotope tracing, infrared spectroscopy, X-ray absorption near-edge structure, X-ray photoemission spectroscopy and so on. The advantages and limitation of these techniques are discussed in the following sections in the view of the aim of this thesis.

1.2 Probe Molecules and Reactions for Dynamic State of Catalysts

All kinds of catalytic reaction could be, in principle, probes of certain catalyst. A probe reaction must, however, have at least one significant alternative in its characteristics to give information of surface state. It may be the activity, chemoselectivity, regioselectivity, stereoselectivity, or the other kinds of selectivity (dimerization or dehydrogenation, isotope distributions, and so on). The experimental procedure depends on what the alternative is. And it must be carefully chosen for defining the structure and properties of surface or metal particles of the catalyst. Another interest is the factor ruling the phenomena arising between surface structure/properties and elementary processes. Both aspects are undivided and should be discussed at a time in the investigation of the chemical reaction on the heterogeneous surface. This is an another expression of the reaction mechanism including catalyst surface.

Ethanol dehydration/dehydrogenation which gives some information on the active site of acid catalysts and generation

of dialkylbenzene in zeolite determining the size of cavities are famous and reported elsewhere. As for metal catalysts, hydrogenation-related reactions are favorable and all of the catalytic reactions in this thesis belongs to them.

H_2-D_2 exchange reaction

The information this reaction includes is the ability of the catalyst to adsorb hydrogen as dissociative form. The mechanism of this most simple catalytic reaction has been investigated for itself [14-17] but it seems to show its worth during the hydrogenation of the unsaturated compound. Whether it is the rate-determining or not, whether it competes in adsorption with a reactant or not, whether the site is the same as that of hydrogenation or not --- these are questions which result of this reaction may answer.

The results of the reaction appear everywhere in the thesis.

CH_2=CH_2 deuteration

Studies on ethane formation accompanied with the adsorbed state may present a typical development of reaction mechanism of heterogeneous catalysis. [18-25] The adsorbed state of ethene has been agreed with including π-, di-σ-states and the other species on the surface of metals. These adsorbates can get hydrogen to be half-hydrogenated states and another H addition makes them ethane. Quasi-equilibrium forms between associative state and half-hydrogenated state under room temperature (Scheme 1.1). This is generally accepted reaction scheme on transition metal catalyst so far.

Isotope distribution of deuterated ethanes is determined by the balance of the life time of CH_2-CH_2(ad) and CH_2-CH_2D(ad) in

their quasi-equilibrium and surface ratio of D/H. The latter is determined by the adsorption competition of $CH_2=CH_2$ and D_2 and quasi-equilibrium. The products are often smeared on metallic

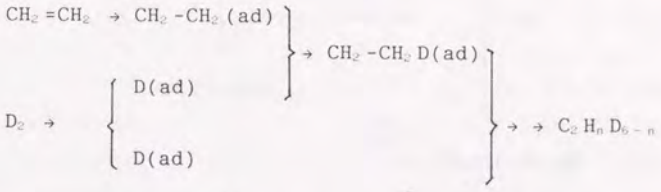

Scheme 1.1 Intermediates and their conversions in ethene-deuterium reaction.

catalysts. Ni produces d_6-ethane preferentially at the initiation of $D_2-CH_2=CH_2$ reaction [19] while Rh, Ir and Pt produce d_2-ethane preferentially [26]. Several metal oxide catalysts also activate ethene to form ethane but the shuffling of deuterium and hydrogen does not occur during $D_2-CH_2=CH_2$ reaction; produced ethane is almost exclusively CH_2DCH_2D in the reaction. [27] When reduction temperature increases in the preparation of an active metal oxide catalyst, metallic active site gradually generates. Accordingly the distribution of deuterated ethane should be spread, that is, d_6- and d_1-ethanes come to form. This offers possibility of characterizing the degree and extent of surface reduction. [28]

$CH_2=CHCHO$ hydrogenation

Acrolein (2-propenal) has two kinds of unsaturated bonds, C=C and C=O, and, consequently, its chemoselectivity of hydrogenation can be a probe. Usual network of the conversion of it is illustrated in Scheme 1.2. 1-Propanal, CH_3CH_2CHO, is more stable and is a

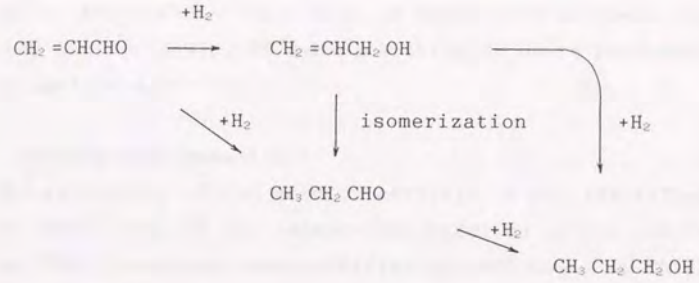

Scheme 1.2 Acrolein hydrogenation network.

preferable product in equivalent molar hydrogen addition. The reaction intermediates are expected from the extrapolation of the mechanism of ethene hydrogenation, i.e., C-C and/or C-O associative mechanism. Conjugated coordination, η^4(C-C-C-O), has been reported in the group VIII metal complex [29] and this kind of adsorption is possible also on metal surfaces.

Acrolein has two conformers; 2 % is *s-cis* and 98 % is *s-trans* at room temperature. The geometry of atomic arrangement (r_s structure) was determined by microwave spectroscopy [30]. Figure 1.1 illustrates molecular structure of these two isomers. It is to be noted that **C3-H7** bond in *s-cis*-acrolein is manifestingly long (1.098 A) comparing with *s-trans*-isomer (1.090 A) or ethene (1.086 A, r_e structure). This offers enough reason for high reactivity of **C3-H7** dissociation or substitution of **H7** hydrogen of η^4(C-C-C-O) adsorbate, which is likely to coordinate as *s-cis*-conformation. Reaction intermediates and their conversion of D_2-CH_2=CHCHO reaction were already discussed [31] before the determination of the molecular structure of *s-cis*-

acrolein. They concluded that the exchange of terminal hydrogen (H7 or H8, not distinguished) of deuterated acrolein resulted from intramolecular H7 hydrogen shift to O4 through substitution by surface deuterium.

CH_2=CHX hydrogenation

The reactivity of C=C bond in acrolein is not identified to that of ethene even in the independent reaction of C=C and C=O due to the C=C electronic state modified by carbonyl. In this context, all the olefins have different behavior in hydrogenation because electronic states, especially LUMO and HOMO, are perturbed by substitutional group, X. [32] Thus the interaction between metal and carbon-carbon double bond, which is usually expressed electron donation and/or backdonation, can be probed by the electron withdrawal character of X. It has been reported that linear free energy relationship (LFER) is observed between Hammett's σ and dissociative constant related to metal-C=C bond in mononuclear group VIII metal complexes in homogeneous system. [33-35] This relation is also valid in metal particle system in principle since the width of metal d-band is usually narrow. In usual hydrogenations on metal, olefinic molecules are compete with hydrogen in adsorption but they are stronger than hydrogen at enough low temperature. It is likely that LFER influences on the rate and kinetics of hydrogenations.

In a probing reaction, X needs its stability in the hydrogenation condition. Preferable set of CH_2=CHX is chosen as follows;

(CH_2=CH_2	ethene)
CH_2=$CHCH_3$	propene
CH_2=$CHCF_3$	3,3,3-trifluoropropene

$CH_2=CHCOCH_3$ methylvinylketone

$CH_2=CHCN$ acrylonitrile

whose reactivity of X themselves and C-X bonds are lower than CHO in general. Multi-substituted ethene might be possible but in this case the problems happens in the stereochemical hindrance and/or the lack of site of the exchange reaction between H and surface D.

There are other superior probing reactions of metal surface, such as regioselectivity of methylcyclopentane hydrogenolysis [36-39] and selectivity of propene-deuterium exchange [40-41].

1.3 Hydrogenation Kinetics of Heterogeneous Surface

Kinetic investigation is a primary test for the reaction mechanism and appears everywhere in this thesis. Catalytic reactions on a heterogeneous surface need correction and addition to the kinetics of uniform surfaces. General consideration might be useful for understanding of the description in the following chapters.

The simplest case is that the catalytic reaction involves no transfer of adspecies among different regions of surface and no interactions among them. The rate of formation, r, is represented by the sum of the rate of each region, r_i.

$$r = \Sigma r_i \qquad (1.1)$$

Selectivity and isotope distributions should be considered on the base of this equation. (1.1) is very simple but includes an important criterion for the mechanism and active sites. (1.1) can be transformed into Arrhenius type equation with activation energy E_i and preexponential factor A_i.

$$r = \Sigma A_i \exp(-E_i x/R),\ x = T^{-1} \quad (1.2)$$

Differential of (1.2) defines the form of Arrhenius plots.

$$(dr/dx) = -\Sigma (E_i/R) A_i \exp(-E_i x/R) < 0 \ , \text{ if } E_i > 0 \quad (1.3)$$

$$(d^2 r/dx^2) = \Sigma (E_i/R)^2 A_i \exp(-E_i x/R) > 0 \ , \text{ if } E_i > 0 \quad (1.4)$$

Thus the reaction with positive apparent activation energy gives convex and monotonous decreasing function in Arrhenius diagram. If a break appears in an Arrhenius plot, it must be contrary to the case of the shift of rate-determining step in a serial consequence reaction as illustrated in Figure 1.2. The possibility of this type of break should be always noted.

The situation is more complicated in the reaction with transfer of adspecies among the regions which play a different role in the whole reaction. The discussion here is restricted to the typical hydrogenation of unsaturated molecules, i.e., associative hydrogenation. Usual scheme of associative mechanism on an uniform surface is as follows;

$$R + X \rightarrow RX \quad (1.5)$$

$$H_2 + 2X \rightarrow 2HX \quad (1.6)$$

$$RX + HX \rightarrow RHX + X \quad (1.7)$$

$$RHX + HX \rightarrow PX + X \quad (1.8)$$

$$PX \rightarrow P + X \quad (1.9)$$

where R is unsaturated compound, P is a product and X is active site. The rate is expressed as

$$r = k_6 P_{H_2} [X]_0^2 / (1+K_5 P_R)^2 \quad (1.10)$$

in (1.6) rate-determining,

$$r = k_7 K_5 K_6^{1/2} P_{H_2}^{1/2} P_R [X]_0^2 / (1+K_R P_R + K_6^{1/2} P_{H_2}^{1/2})^2 \quad (1.11)$$

in (1.7) rate-determining or

$$r = k_8 K_5 K_6 K_7 P_{H_2} P_R [X]_0^2 / (1+K_R P_R + K_6^{1/2} P_{H_2}^{1/2} + K_5 K_7 K_6^{1/2} P_{H_2}^{1/2} P_R)^2 \quad (1.12)$$

in (1.8) rate-determining where k_i and K_i are constants and P_{H_2}

and P_R are partial pressure of hydrogen and unsaturated compound. $[X]_0$ is the number of active site.

If elementary reactions like (1.5)∼(1.9) occur active site X and Y, several cases are possible and the formation rate of P should be given for each case. Typical cases are listed as follows with rate-equations.

I. Adsorption sites are different and atomic hydrogen diffuses into R's site.

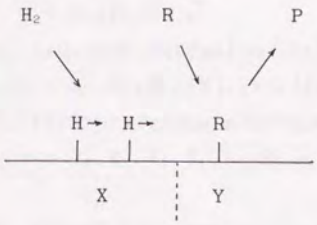

$$R + Y \rightarrow RY \qquad (1.13)$$

$$H_2 + 2X \rightarrow 2HX \qquad (1.14)$$

$$HX + Y \rightarrow HY + X \qquad (1.15)$$

$$RY + HY \rightarrow RHY + Y \qquad (1.16)$$

$$RHY + HY \rightarrow PY + Y \qquad (1.17)$$

$$PY \rightarrow P + Y \qquad (1.18)$$

1. hydrogen adsorption, (1.14), rate-determining

$$r = k_{14} P_{H2} [X]_0^2 \qquad (1.19)$$

2. hydrogen diffusion, (1.15), rate-determining

$$r = k_{15} K_{14} P_{H2} [X]_0 [Y]_0 / (1+K_{14} P_{H2})(1+K_{13} P_R) \qquad (1.20)$$

3. first hydrogen addition, (1.16), rate-determining

$$r = k_{16} K_{13} K_{15} K_{14}^{1/2} P_{H2}^{1/2} P_R [Y]_0^2 / (1+K_{15} K_{14}^{1/2} P_{H2}^{1/2} + K_{13} P_R)^2 \qquad (1.21)$$

4. second hydrogen addition, (1.17), rate-determining

$$r = k_{17} K_{13} K_{14} K_{15}^2 K_{16} P_{H2} P_R [Y]_0^2 / (1+K_{13} P_R + K_{15} K_{14}^{1/2} P_{H2}^{1/2} + K_{13} K_{15} K_{16} K_{14}^{1/2} P_{H2}^{1/2} P_R)^2 \qquad (1.22)$$

II. Adsorption sites are different and one atomic hydrogen diffuses into R's site and another hydrogen addition occurs at

the boundary.

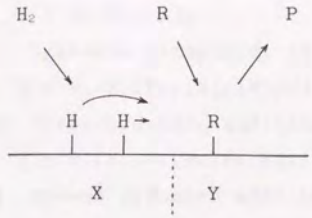

$$R + Y \rightarrow RY \quad (1.23)$$

$$H_2 + 2X \rightarrow 2HX \quad (1.24)$$

$$HX + Y \rightarrow HY + X \quad (1.25)$$

$$RY + HY \rightarrow RHY + Y \quad (1.26)$$

$$RHY + HX \rightarrow PY + X \quad (1.27)$$

$$PY \rightarrow P + Y \quad (1.28)$$

1. hydrogen adsorption, (1.24), rate-determining

$$r = k_{24} P_{H2} [X]_\emptyset^2 \quad (1.29)$$

2. hydrogen diffusion, (1.25), rate-determining

$$r = k_{25} K_{24} P_{H2} [X]_\emptyset [Y]_\emptyset / (1+K_{24} P_{H2})(1+K_{23} P_R) \quad (1.30)$$

3. first hydrogen addition, (1.26), rate-determining

$$r = k_{26} K_{23} K_{25} K_{24}^{1/2} P_{H2}^{1/2} P_R [Y]_\emptyset^2 / (1+K_{25} K_{24}^{1/2} P_{H2}^{1/2} + K_{23} P_R)^2 \quad (1.31)$$

4. second hydrogen addition, (1.27), rate-determining

$$r = k_{27} K_{23} K_{24}^{3/2} K_{25} K_{26} P_{H2}^{3/2} P_R [X]_\emptyset [Y]_\emptyset / (1+K_{23} P_R + K_{25} K_{14}^{1/2} P_{H2}^{1/2} + K_{23} K_{25} K_{26} K_{24}^{1/2} P_{H2}^{1/2} P_R)(1+K_{24} P_{H2}) \quad (1.32)$$

III. Adsorption sites are different and one hydrogen is added at the boundary and another hydrogen diffuses into R's site.

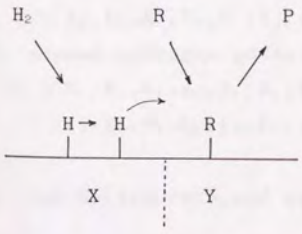

$$R + Y \rightarrow RY \quad (1.33)$$

$$H_2 + 2X \rightarrow 2HX \quad (1.34)$$

$$HX + Y \rightarrow HY + X \quad (1.35)$$

$$RY + HX \rightarrow RHY + X \quad (1.36)$$

$$RHY + HY \rightarrow PY + Y \quad (1.37)$$

$$PY \rightarrow P + Y \quad (1.38)$$

1. hydrogen adsorption, (1.34), rate-determining

$$r = k_{34} P_{H2} [X]_0^2 \qquad (1.39)$$

2. hydrogen diffusion, (1.35), rate-determining

$$r = k_{35} K_{34} P_{H2} [X]_0 [Y]_0 / (1+K_{34} P_{H2})(1+K_{33} P_R) \qquad (1.40)$$

3. first hydrogen addition, (1.36), rate-determining

$$r = k_{36} K_{33} K_{34} P_{H2} P_R [X]_0 [Y]_0 / (1+K_{33} P_R)(1+K_{34} P_{H2}) \qquad (1.41)$$

4. second hydrogen addition, (1.37), rate-determining

$$r = k_{37} K_{33} K_{34} K_{35} K_{36} P_{H2} P_R [Y]_0^2 / (1+K_{33} P_R + K_{35} K_{34}^{1/2} P_{H2}^{1/2} + K_{33} K_{36} K_{34}^{1/2} P_{H2}^{1/2} P_R)^2 \qquad (1.42)$$

IV. Adsorption sites are different and hydrogen is added at the boundary.

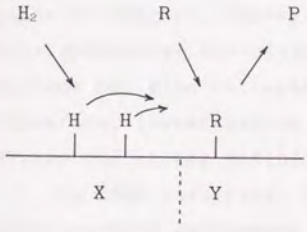

$$R + Y \rightarrow RY \qquad (1.43)$$

$$H_2 + 2X \rightarrow 2HX \qquad (1.44)$$

$$RY + HX \rightarrow RHY + X \qquad (1.45)$$

$$RHY + HX \rightarrow PY + X \qquad (1.46)$$

$$PY \rightarrow P + Y \qquad (1.47)$$

1. hydrogen adsorption, (1.44), rate-determining

$$r = k_{44} P_{H2} [X]_0^2 \qquad (1.48)$$

2. first hydrogen addition, (1.46), rate-determining

$$r = k_{45} K_{43} K_{44} P_{H2} P_R [X]_0 [Y]_0 / (1+K_{43} P_R)(1+K_{44} P_{H2}) \qquad (1.49)$$

3. second hydrogen addition, (1.47), rate-determining

$$r = k_{46} K_{43} K_{44} K_{45} P_{H2} P_R [X]_0 [Y]_0 / (1+K_{43} P_R + K_{43} K_{45} K_{44}^{1/2} P_{H2}^{1/2})(1+K_{44}^{1/2} P_{H2}^{1/2}) \qquad (1.50)$$

k_i and K_i are rate and equilibrium constants of corresponding

elementary steps, respectively. P_i is partial pressure of species i. $[X]_\emptyset$ and $[Y]_\emptyset$ are the area or the number of active sites of corresponding region. These cases assumed that one hydrogen atom occupied the same number of active site of an olefin. If it is smaller, the power, n, of $[X]_\emptyset^n/(\cdots\cdots)^n$ should be smaller in the equations (1.10)~(1.12). The same correction holds true for the other equations. Experimental determination of n is not easy and, therefore, the qualitative discussion seems safer in applying equations above.

Rate expression as a function of partial pressure of reactants makes it possible to identify the rate-determining step in principle. It is, however, sometimes difficult to interpret dispersed experimental spots. The other approach is noting $[X]_\emptyset$ and $[Y]_\emptyset$. The exemplified cases in I ~ IV have three different kinds of factors, namely, $[X]_\emptyset^2$, $[Y]_\emptyset^2$ or $[X]_\emptyset[Y]_\emptyset$. Recent physicochemical techniques can not only characterize the state of surface but also estimate and design the area of each region. Therefore, investigation of rate dependence on the area sometimes offers the strong definition of rate-determining step.

In SMSI catalysts, for example, the support migrates on the metal surface as thermal diffusion process when the reduction temperature is enough high. [41] Thus the number of active sites of the migrated support oxide on metal particles, $[Z]_\emptyset$, is presented as a function of reduction time, t_R;

$$[Z]_\emptyset = \alpha t_R^{1/2} \tag{1.51}$$

α is coefficient independent of t_R. That of bare metal surface, $[X]_\emptyset$, is

$$[X]_\emptyset = S_\emptyset - \alpha t_R^{1/2} \tag{1.52}$$

where $S_\emptyset$ is the number of active site of non-covered surface. The peripheral site of a migrated support could offer the special

catalyses and the number of sites is given as

$$[Y]_0 = \beta t_R^{1/4} \tag{1.53}$$

where β is constant. Rates under constant pressure of reactants as a function of t_R differentiate three cases of hydrogenation on SMSI catalyst which is one of typical hydrogenation on heterogeneous surface. That is, the factors appearing in the rate equation, $[X]_0^2$, $[Y]_0^2$ and $[X]_0[Y]_0$, are substituted by (1.51)~(1.53);

$$[X]_0^2 = S_0^2 - 2\alpha S_0 t_R^{1/2} + \alpha^2 t_R \tag{1.54}$$

$$[Y]_0^2 = \beta^2 t_R^{1/2} \tag{1.55}$$

$$[X]_0[Y]_0 = \beta S_0 t_R^{1/4} - \alpha\beta t_R^{3/4} \tag{1.56}$$

The activity of the site on the migrated support is usually low and negligible. (1.54) is monotonously decreasing because $t_R > S_0/2\alpha$ (because of $[X]_0 > 0$) and (1.55) is monotonous increasing while (1.56) has a maximum at $t_R = S_0^2/9\alpha^2$ ($[X]_0 = 2S_0/3$). These three functions are easily distinguishable as shown in Figure 1.3.

Kinetical investigation is essential for the reaction mechanism of catalysis on non-uniform surface in the classical view and the modern view; it is the first test for the site identification for the elementary steps including rate-determining step. In other words, it is possible that the elementary steps and surface heterogeneity bind together through kinetic study.

References

1. for example, G.Ertl, *in* "Chemistry and Physics of Solid Surfaces VIII", R.Vanselow and R.Howe, eds., p.1, Springer Verlag, Berlin, 1990.
2. G.A.Somorjai, "Chemistry in Two Dimensions: Surface", Cornell University Press, 1981.
3. J.K.Strohl, T.S.King, *J.Catal.*, **116**, 540 (1989); *ibid.*, **119**, 441 (1989).
4. N.D.Spencer, R.C.Schoonmaker, G.A.Somorjai, *J.Catal.*, **74**, 129 (1982)., *Nature*, **294**, 643 (1981).
5. S.J.Thomson, *J.Chem.Soc., Faraday Trans. 1*, **83**, 1893(1987).
6. B.Imerik, C.Naccache, G.Coudurier, H.Praliaud, P.Meriaudeau, G.A.Martin, J.C.Verdrine, *eds.*, "Metal-Additive and Metal-Support Effects in Catalysis", Elsevier, Amsterdam, 1982.
7. G.L.Haller, D.E.Resasco, *Adv.Catal.*, **36**, 173 (1989).
8. R.Burch, *in* "Hydrogen Effects in Catalysis", P.Zoltan and P.G.Menon, eds., Dekker, New York, 1988.
9. S.J.Tauster, S.C.Fung, R.T.K.Baker, J.A.Horsley, *Science*, **211**, 1121 (1981).
10. S.J.Tauster, *Acc.Chem.Res.*, **20**, 389 (1987).
11. R.T.K.Baker, S.J.Tauster, J.A.Dumesic, "Strong Metal-Support Interactions", *ACS Symposium Series* 298. American Chemical Society, Washington DC, 1986.
12. E.Guglielminotti, *J.Catal.*, **120**, 287 (1989).
13. P.Basu, D.Panayotov, J.T.Yates,Jr., *J.Am.Chem.Soc.*, **110**, 2074 (1988).
14. K.F.Bonhoeffer, A.Farkas, *Z.Phys.Chem.*, **12B**, 231 (1931).
15. E.K.Rideal, *Proc.Cambridge Phil.Soc.*, **35**, 130 (1934).
16. K.E.Lu, R.R.Rye, *Surf.Sci.*, **45**, 677 (1974).

17. M.Salmeron, R.J.Gale, G.A.Somorjai, *J.Chem.Phys.*, **67**, 5324 (1977).
18. J.Horiuti, M.Polanyi, *Trans.Faraday Soc.*, **30**, 1164 (1934).
19. J.Turkevich, E.Bonner, D.O.Schissler, A.P.Irsa, *Discuss. Faraday Soc.*, **8**, 325, (1950).
20. A.Farakas, L.Farakas, E.K.Rideal, *Proc.R.Soc.London, Ser A*, **146**, 630 (1934).
21. T.P.Beebe,Jr., J.T.Yates,Jr., *J.Phys.Chem.*, **91**, 254 (1987).
22. D.B.Zax, C.A.Klug, C.P.Slichter, J.H.Sinfelt, *J.Phys.Chem.*, **13**, 5009 (1989).
23. A.L.Backman, R.I.Masel, *J.Phys.Chem.*, **94**, 5300 (1990).
24. E.Yagasaki, A.L.Backman, R.I.Masel, *J.Phys.Chem.*, **94**, 1066 (1990).
25. S.B.Mohsin, M.Trenary, H.J.Robota, *J.Phys.Chem.*, **92**, 5229 (1988).
26. G.C.Bond, J.J.Phillipson, P.B.Wells, J.W.Winterbottom, *Trans.Faraday Soc.*, **60**, 1847 (1964); *ibid.*, **62**, 443 (1966)
27. W.C.Conner, R.J.Cokes, *J.Phys.Chem.*, **73**, 2436 (1969).
28. P.Nazario, A.Brenner, *Proceedings of 10th Int. Congr. Catal.*, 1988, p.1020.
29. H.P.Fritz, G.N.Schrauzer, *Chem.Ber.*, **94**, 650 (1961).
30. C.E.Blom, G.Grassi, A.Bauder, *J.Am.Chem.Soc.*, **106**, 7427 (1984).
31. R.Touroude, *J.Catal.*, **65**, 110 (1980).
32. I.Flemming, "Frontier Orbitals and Organic Chemical Reactions", Chapter 2, John Wiley & Sons, London, 1976.
33. C.A.Tolman, *J.Am.Chem.Soc.*, **96**, 2780 (1974).
34. T.Yamamoto, A.Yamamoto, S.Ikeda, *J.Am.Chem.Soc.*, **93**, 3360 (1971).
35. R.Cramer, *J.Am.Chem.Soc.*, **86**, 217 (1964).

36. V.Ponec, *in* "The Chemistry and Physics of Solid Surfaces and Heterogeneous Catalysis", P.A.King and D.P.Woodruff eds., vol.4, Elsevier, Amsterdam, 1982.
37. B.J.Tatarchuk, J.A.Dumesic, *J.Catal.*, **70**, 308 (1981).
38. J.B.F.Anderson, R.Burch, J.A.Cairns, *J.Catal.*, **107**, 351 (1987).
39. R.J.Fenoglio, G.M.Nuñez, D.E.Resasco, *J.Catal.*, **121**, 77 (1990).
40. T.Kondo, S.Saito, K.Tamaru, *J.Am.Chem.Soc.*, **96**, 6857 (1974).
41. R.D.Resasco, G.L.Haller, *J.Catal.*, **82**, 279 (1983).

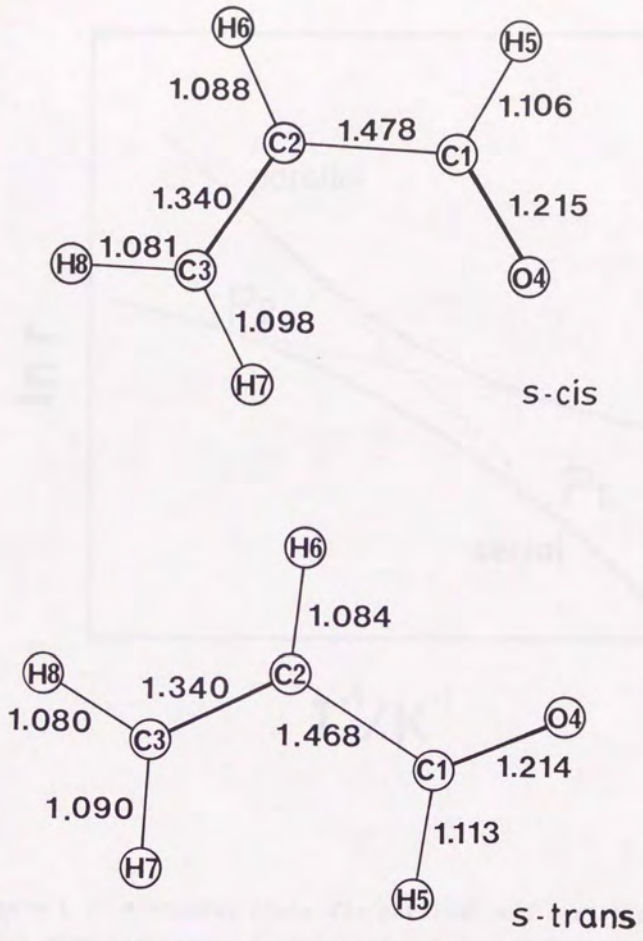

Figure 1.1 Atomic numbering scheme and bond lengths for *s-cis* acrolein and *s-trans*-acrolein.

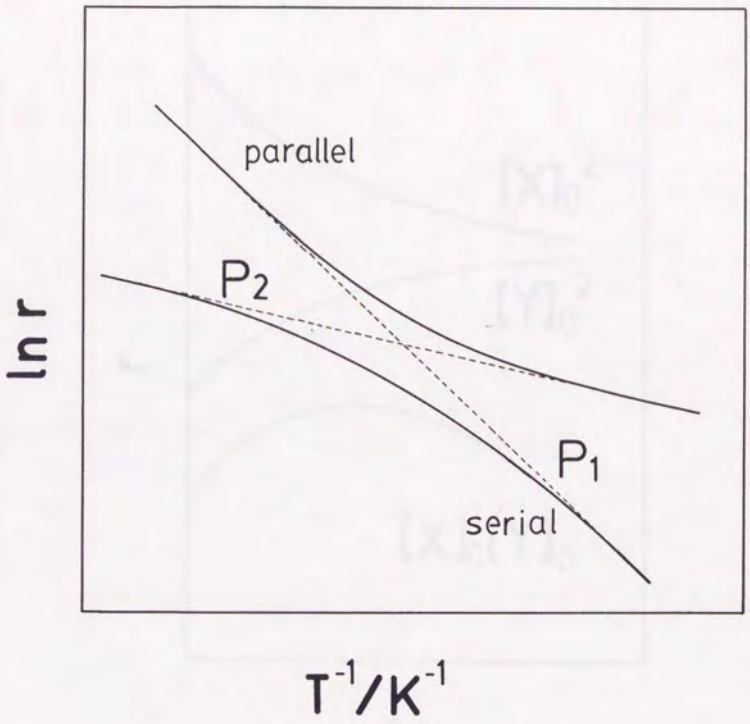

Figure 1.2 Arrhenius plots for parallel and serial processes of multi-step reaction. Broken lines of P_1 and P_2 are elementary steps. Observed Arrhenius plots for parallel reaction-system, such as multi-active sites, is presented as upper line and serial step-system, such as adsorption → P_1 → P_2 → desorption, is presented as lower line.

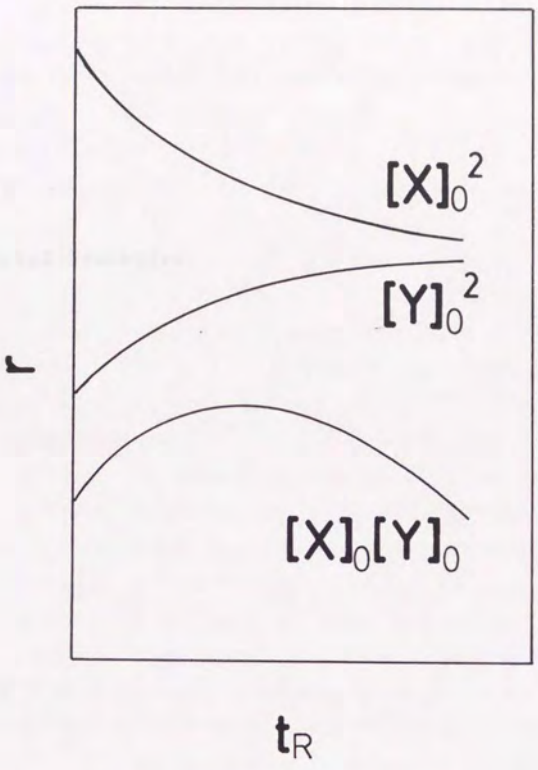

Figure 1.3 Hydrogenation rate of possible reaction types on SMSI catalyst. Rates are represented by reduction time of catalysts, t_R. $[X]_0$ and $[Y]_0$ appear in the rate equations and represent the number of active sites of different region. It is possible to distinguish the reaction mechanism by interpretation of the shape of $r(t_R)$.

Chapter 2

Experimental Procedure

Each chapter has a section about methods of experiments and data analysis. Nevertheless, it is still useful for understanding the experiments and for the interpretation of the results to describe general aspect of the techniques.

2.1 Catalyst Preparation and Set-ups for Catalytic Reactions

All catalysts were prepared by impregnation method of aqueous solution of metal salts, which was not expected to give defined molecular structure like attached metal catalysts [1]. These "non-tailored catalysts" are rather preferable to the aim; the surface heterogeneity can not be within an expect. Reagents are described in each chapter.

Particle size, which was to be average size, was estimated by transmission electron microscopy (TEM) and hydrogen adsorption measurement. Data obtained by these two methods can be related by ref 2. If the gap is observed between two, an extraordinary effect, such as abnormal particle shape or poisoning, should be taken into account. Catalytic reactions were carried out below ambient pressure in an closed circulating system. (dead volume: 150 cm^3) The background pressure was 10^{-4} Pa. Gas chromatograph (GC-6A, Shimadzu, with TCD detector) and quadrupole mass spectrometer (AQA-100R, ANELVA) connected to it in order to determine the gas composition of the system. Each sampling volume was 2 %. Data were accumulated with chromatopac (C-R3A, Shimadzu) for GC-6A and floppy discs in personal computer (PC-9801UX21, NEC) through GP-IB interface.

2.2 Product Analysis

Products were separated chemically and analyzed quantitatively with gas chromatography. Separating columns used were Molecular Sieve 5A, VZ-10 and PEG-1500. Product range were within 10^4, which is well in the TCD linearity. Isotopes were distinguished by quadrupole mass spectrometry after separation by a column. The identification of the isotopes should be commented.

Ethane and Ethene

Ethanes and ethenes were ones of the first compounds distinguished isotopically in catalytic chemistry. [3] Methods which was applied in the research is valid for most cases still today.

Isotopic effects appeared between C-D and C-H cleavage are negligible. Thus the branching patterns of all ethanes, C_2H_6, C_2H_5D, $C_2H_4D_2$, $C_2H_3D_3$, $C_2H_2D_4$, C_2HD_5 and C_2D_6 are obtained through the analysis of fragmentation of C_2H_6. Mass spectrum charts of the reaction gas are analyzed through the fitting of all these patterns. Isotopes of ethene are analyzed by a similar way.

This method can be applied for all compounds, not only for hydrocarbons, in principle. There is an isotope effect for the aldehydic hydrogen cleavage, that is, $p_D/p_H = 0.95$ where $p_D = (RC{=}O)^+/(RCDO)^+$ and $p_H = (RC{=}O)^+/(RCHO)^+$, which was detected in the d_0-propanal/1-d_1-propanal after the exchange reaction of D_2-CH_3CH_2CHO on Pd/SiO_2. The formation of CH_3CH_2CDO was confirmed by infrared spectroscopic detection of the shift of aldehydic hydrogen.

Oxygen Containing Molecules

The atomic numbering of C_3-oxygenates hereafter is ^3C-^2C-^1C-O or

$_{\gamma}C\text{-}_{\beta}C\text{-}_{\alpha}C\text{-}O$.

Some model compounds are chosen for the molecular ion cleavages.

(1)$CH_2=CHBr$ for $CH_2=CH^+$ (distributed as 24 ~ 27 in m/z)

(2)CH_3CH_2Br for $CH_3CH_2^+$ (distributed as 24 ~ 29 in m/z)

(3)$CH_2=CHCH_2Br$ for $CH_2=CHCH_2^+$ (distributed as 36 ~ 41 in m/z) and

(4)$CH_2=CHCH=CH_2$ for $CH_2=CHCH^+$ (distributed as 36 ~ 40 in m/z).

The last distribution chart is obtained with subtraction by that of (3) from the law distribution of corresponding region. Mass spectrum charts are divided for four regions as for each compound; m/z = 12 ~ 23, m/z = 24 ~ 35, m/z = 36 ~ 51 and m/z = 52 ~ represent region I, region II, region III and region IV, respectively. Molecular ions under consideration belong to one region. Molecular ions and ions with no skeleton cleavages appear in Region IV. Region II is dominated by the α-β cleavage due to the small contribution of β-γ and O-α simultaneous cleavage. As for region III, both of β-γ and O-α cleavages contribute.

The analysis of acrolein is based on five ions and their fragment ions, $CH_2=CH^+$, $CH=O^+$ (Region II), $CH_2=CHCH^+$, $CH-CH=O^+$ (Region III) and $CH_2=CHCH=O^+$ (Region IV). The spectrum pattern of m/z = 24 ~ 27 agrees that of (1). The fragmentation of $CH_2=CHCH^+$ is assumed to be the same as (4) and the subtraction of $CH_2=CHCH^+$ pattern from the chart of region III offers the pattern of $CH-CH=O^+$. The isotopes of every ion and fragment is calculated in the similar way with ethane and ethene. The spectra of the reaction gas under investigation are divided into the each isotopic species in each region to determine the isotope distribution of ions. The number of deuterium sited on each carbon is determined as follows;

α-d(aldehydic deuterium) = $n_{\alpha\beta\gamma} - n_{\beta\gamma}$ (or = $n_{O\alpha}$) (2.1)

β-d = $n_{O\alpha\beta} - n_{O\alpha}$ (2.2)

γ-d(terminal deuterium) = $n_T - n_{O\alpha\beta}$ (2.3)

where $n_{(\ldots)}$ is the number of deuterium in the skeleton $^{\gamma}C-^{\beta}C-^{\alpha}C-O$ and its fragments. n_T represents the total number of deuterium included in the molecule, i.e., equals to $n_{O\alpha\beta\gamma}$. Isotope distribution of ions is attributed to that of molecule.

Propanal is considered with dividing the chart into region I, region II and region IV which reflects β-γ cleavage (CH_3^+), α-β cleavage ($CH_3CH_2^+$ and $CH{=}O^+$, the former is assumed to be the same as (2) and the latter is derived by subtraction of the fragmentation of the former) and the molecular ion ($CH_3CH_2CH{=}O^+$), respectively. The pattern of region I is almost the same as that of CH_3Br. The number of deuterium on each carbon atom and oxygen is calculated as follows;

α-d(aldehydic deuterium) = $n_{O\alpha}$ (2.4)

β-d = $n_{\beta\gamma} - n_\gamma$ (2.5)

γ-d(terminal deuterium) = n_γ (2.6)

The analysis of allyl alcohol needs region II, region III and region IV, which reflects α-β cleavage ($CH_2{=}CH^+$, CH_2OH^+), O-α and β-γ cleavage ($CH_2{=}CHCH_2^+$ and $CHCH_2OH^+$, respectively, the former is assumed to be the same as (3) and the latter is derived by subtraction of the fragmentation of the former), and molecular ion, respectively. Mass region of m/z = 24 ~ 27 is almost the same as that of acrolein and (1). The number of deuterium on each carbon atom and oxygen is calculated as follows;

O-d(alcoholic deuterium) = $n_T - n_{\alpha\beta\gamma}$ (2.7)

α-d = $n_{\alpha\beta\gamma} - n_{\beta\gamma}$ (2.8)

β-d = $n_{O\alpha\beta} - n_{O\alpha}$ (2.9)

γ-d(terminal deuterium) = $n_T - n_{O\alpha\beta}$ (2.10)

These analyses are confirmed by mass spectrum charts of several compounds prepared or purchased, such as $CH_3CH_2CD{=}O$ and $CH_2{=}CHCH_2OD$. The maximum difference was ca. 20 %. This offers errors and confidence of determination of isotope distributions by means of the mass spectra analyses.

2.3 Spectroscopy

Spectroscopic techniques are widely applied to catalyst characterization and reaction dynamics on solid surface today. Infrared spectroscopy (IR) is one of the most prevailed tools in laboratory and X-ray photoemission spectroscopy (XPS) is also available everywhere. On the other hand, X-ray absorption spectroscopy (XAS) usually needs a large facility, synchrotron, as a light source in order to gain good spectra. It was necessary in the experiment of following chapters that X-ray absorption near-edge structure (XANES) were measured at Photon Factory of National Laboratory for High Energy Physics (KEK-PF).

The absorption by the molecular vibration of adsorbates on metal catalysts is detectable with IR spectrometer. In the following chapters FT/IR-7000 (JASCO) was used with 2 cm^{-1} of resolution in order to elucidate the kinds of adsorbates and their reactivity. The catalysts were molded into disks after calcination and mounted in the quartz-made IR cell connected with a gas circulating system.

XPS is a probe detecting kinetic energy of electron emitted from the material. The transmission ability of electron is low and it makes XPS surface-sensitive. This is quite preferable in some cases but at the same time it is impossible to use in the

gas reactants, which constructs a large barrier for the study of catalytic reaction. Anyway, XPS is a very convenient tool for the surface composition of the catalyst just before reactions.

XAS is a photon-using probe and, consequently, it can be a investigating tool for catalysts under gas of large pressure. XANES clarify the stereochemistry of the local structure of an element under discussion and the electronic state of the element when its data are analyzed adequately. Especially white lines of transition metals reflect small change of the electronic state of atoms. [4] XAS is not surface sensitive and detect the atoms in largest number among various states or the average state of the atoms. This sometimes offers crucial problems in the interpretation of spectra in the study of heterogeneous catalysts.

References

1. Y.Iwasawa, eds. "Tailored Metal Catalysts", Chapter 1, D.Reidel Publishing Co., Dordrecht, 1986.
2. R.Anderson, "Structure of Metallic Catalysts", P.361, Academic Press, New York, 1975.
3. J.Turkevich, E.Bonner, D.O.Schissler, A.P.Irsa, *Discuss. Faraday Soc.*, 8, 325 (1950).
4. J.C.J.Bart, *Adv.Catal.*, 34, 203 (1986).

Chapter 3

Local Reaction Environments and their Properties for Ethene Deuteration on the Surfaces of SMSI Catalysts

Catalysis by noble metals supported on TiO_2 or Nb_2O_5 has attracted considerable interest in relation to strong metal-support interaction (SMSI) phenomena as well as surface chemistry, in order to inspect physicochemical properties controlling metal catalysis. [1, 2] Numerous authors have pointed out the characteristic features of SMSI states of catalysts, such as a reduction in the hydrogenation activity for alkenes, [3, 4] a drastic decrease in hydrogenolysis activity [4, 5] and a unique product distribution in CO hydrogenation. [6, 7] These changes or modifications in catalysis are believed to derived from the presence of TiO_x or NbO_x that has migrated onto the metal surface, and hence the large part of SMSI catalysis is inclined to be due to a blockage by TiO_x or NbO_x on the metal surface, [5, 8-12] the destruction of the ensemble required for activity, [5] or an adsorbate-Ti^{n+} interaction in the periphery of migrated TiO_x, which is assumed to be an important intermediate for enhanced hydrogenation. [13-15]

Catalytic reactions are generally composed of several surface processes (such as adsorption or desorption, the diffusion/transport of adsorbates, and surface reactions in which more than one adsorbed species participate in) which are affected by the structures and environments at the surface in a different manner. Catalysis by SMSI catalysts, therefore, includes the interaction between active site and reaction intermediates, the relationship between surface processes and specific structures/environments on the metal surfaces, and the transport of adsorbates and catalyst (TiO_x or NbO_x).

These physical and chemical (electronic) factors are likely to be common among metal catalyses involving promoters. A study of catalysis by SMSI catalysts showing characteristic features

may provide a deeper understanding of the essential factors involved in metal catalyses and the reaction environments on metal surfaces, in addition to information on the development of active multifunctional metal catalysts. This chapter presents an investigation of the role of NbO_x species in ethene deuteration on Ir/Nb_2O_5 and Rh/Nb_2O_5 which shows that NbO_x diffused onto the metal surface brings about not only a modification of the stability of the reaction intermediates but also a differentiation between two reaction environments with different local ratios of hydrogen/deuterium on the surface.

3.1 Experimental

Supported rhodium and iridium catalysts were prepared by conventional impregnation of Nb_2O_5 with an aqueous solution of $RhCl_3 \cdot 3H_2O$ or $IrCl_3 \cdot 1.5H_2O$(Soekawa chemical, Co., Ltd. 99.9 %) followed by drying for 3 h at 393 K and calcination for 2 h at 773 K. The metal loadings were 2.0 and 2.4 wt% for Rh/Nb_2O_5 and Ir/Nb_2O_5, respectively. The catalysts were pretreated with oxygen for 1 h at 673 K, followed by evacuation for 30 min, and reduced for 1 h at 433 K for the low-temperature reduced (LTR) catalyst or at 773 K (for high-temperature reduced (HTR) catalyst, followed by evacuation for 30 min *in situ* before each catalytic reaction. The particle sizes of the supported metals was estimated by hydrogen chemisorption at room temperature, transmission electron microscopy (TEM) and X-ray diffraction (XRD). No surface chloride was detected by XPS on the reduced catalyst.

Ethene, purchased from Takachiho Trading Co., Ltd. (99.9%), was purified by freeze-thaw cycles. Hydrogen and deuterium gases

of research grade were further purified through a molecular-sieve trap at 77 K.

The reactions of D_2 with ethene, H_2 with ethene and a D_2-H_2 mixture with ethene were carried out in a closed circulating system (dead volume 150 cm^3) in the temperature range 210-321 K. A small portion of the reaction gas during the reaction was analysed at intervals by gas chromatography using a VZ-10 column. Deuterated products in the D_2-ethene reaction were also analysed by mass spectrometry after the separation with VZ-10.

3.2 Results and Discussion

Kinetic Behavior

The average particle sizes of the catalysts determined by H_2 chemisorption, TEM and XRD are shown in Table 3.1. The H/M of HTR for both Rh/Nb_2O_5 and Ir/Nb_2O_5 were almost zero compared with those for LTR catalysts, agreed with the literature. Except for this, all values are in good agreement when a 1:1 stoichiometry for H/Rh or H/Ir and a spherical shape were assumed in determining particle sizes by H_2 chemisorption. Significant differences between LTR and HTR catalysts were not found in the TEM and XRD results, which suggests that metal particle sizes were not altered significantly by high-temperature reduction.

Figure 3.1 shows Arrhenius plots for total ethane formation in the D_2-ethene reaction and for HD formation in the D_2-H_2-ethene reaction on Rh/Nb_2O_5. The rates on the LTR catalyst are normalized by H/M to present the turnover frequencies (the activity of each surface Rh atom), where the rates for the HTR catalyst are also normalized on the same scale as that of the LTR catalyst; this avoids the large error derived from the division

of the observed rates by the very small H/M value for HTR. When the rate of ethane formation is compared with that of HD formation, the latter should be reduced to half. The activation energy for HD formation (17 $kJ \cdot mol^{-1}$) on the LTR catalyst was almost the same as that for ethane formation (16 $kJ \cdot mol^{-1}$). These were also similar to those for the HTR catalyst (17 and 17 $kJ \cdot mol^{-1}$). In contrast, on the HTR-Ir/Nb_2O_5 the activation energies for both ethane and HD formation, 3 and 2 $kJ \cdot mol^{-1}$, respectively, were much smaller than those for the HTR-Ir/Nb_2O_5, 22 and 23 $kJ \cdot mol^{-1}$, respectively, as shown in Figure 3.2(a) and (b). The activation energies, 19 and 0 $kJ \cdot mol^{-1}$, for ethane formation in the H_2-ethene reaction on the LTR and HTR catalysts, respectively, were a little smaller than those for ethane formation in the D_2-ethene reaction. The activation energies for HD and ethane formation were almost the same as on Rh/Nb_2O_5, as in Figure 3.2.

The rate-determining step in ethene deuteration under the present experimental condition is suggested to be the dissociation of D_2 because the activation energy for ethane formation agrees well with that of HD formation and it is positive. This holds true for both LTR and HTR catalysts. There is an isotopic effect observed in ethane formation in Figure 3.2, which may be ascribed to the difference between H_2 and D_2 in the energy barrier for the dissociation.

The difference in the activation energies for LTR- and HTR-Ir/Nb_2O_5 observed in Figure 3.2 suggests a large modification of the electronic state of the metal surface by SMSI including the alternation of metal ensembles of active sites. In contrast, a change in activation energy was not observed with Rh/Nb_2O_5 in Figure 3.1, where the SMSI phenomenon with the suppression of

reaction rates appears as 'site blocking' by inactive migrated species in this system.

The difference observed between Ir and Rh may arise from the difference in their particle sizes, or more likely in the strength and morphologic features of their SMSI. Similar differences in SMSI phenomena between different metals has been reported in benzene hydrogenation on Rh/TiO_2 and Pt/TiO_2. [3]

The catalytic activity of the HTR-Ir/Nb_2O_5 catalyst was higher than that of the LTR catalyst for ethane hydrogenation and H_2-D_2 exchange at lower temperatures, in spite of the large decrease in the number of active Ir sites estimated from the H/M. In other words, the Ir sites for hydrogen dissociation are activated by NbO_x that has migrated onto the Ir metal surface in the SMSI state.

Deuteroethane Distribution

The deuterium distributions (relative amounts) in deuteroethane produced at the initial stage of the D_2-ethene reaction are summarized in Tables 3.2 and 3.3. On Rh/Nb_2O_5 the order of population was $d_2 > d_1 \geq d_0$ for LTR catalyst, whereas the order d_0, $d_2 > d_1$ was observed for HTR catalyst. Also in the case of Ir/Nb_2O_5 the population of deuteroethane formed was in the order $d_2 > d_1 > d_0$ for LTR catalyst but d_0, $d_2 > d_1$ for HTR catalyst.

The compositions of H_2, HD and D_2 in the gas phase in the initial stage of the D_2-ethene reaction on Rh/Nb_2O_5 and Ir/Nb_2O_5 are also listed in Tables 3.2 and 3.3. These results demonstrate that the change in the deuterium population of ethane on the LTR and HTR catalysts is not derived from the isotopic compositions of hydrogen in the gas phase during the deuteration of ethene. Very small amounts of deuteroethene comparing to deuteroethane

were observed in the gas phase.

The distribution of deuteroethane reflects the stability of the intermediates of ethane deuteration. The population must be ordered, with $d_2 > d_1 > d_0$ or $d_0 > d_1 > d_2$, when the reaction occurs on only one type of active site with uniform reaction environment. [16-18] In fact, Rh/Al_2O_3 and Ir/Al_2O_3 have been classified as a $d_2 > d_1 > d_0$ group at the reaction temperatures where the rate-determining step is the dissociation of hydrogen. [19, 20] The results for the LTR catalyst agreed with those for Rh/Al_2O_3 and Ir/Al_2O_3; the singular distribution of HTR catalyst suggests that ethane is formed on at least two different kinds of sites. One site may be preferable for the formation of d_2-ethane and the other site for the formation of d_0-ethane. It is natural that the latter sites should be newly generated by the high-temperature prereduction, while the former sites should exist originally on the metal surface and might be modified a little in the SMSI state.

The population of deuteroethane must also reflect the populations of hydrogen and deuterium atoms on the metal surface. In order to obtain structural information in these sites, the rates of the formation of each deuterated species in the D_2-ethene reaction were examined as a function of the high-temperature pretreatment (reduction) time of Rh/Nb_2O_5. (Figure 3.3) There was an optimum value for d_0-ethane formation at *ca.* 50 min. The rate of d_1-ethane formation also had a maximum at *ca.* 45 min reduction time, but the peak was smaller than that for d_0-ethane formation. In the case of d_2-ethane, the rate decreased monotonously with reduction, as shown in Figure 3.3. The slope of the curve for d_0-ethane formation was more gentle than that for the d_2-ethane formation and, consequently, the

reaction rates after the longer prereduction of catalyst were inverted, to form d_0-ethane as a main product. Thus the presence of NbO_x that has migrated onto the metal surfaces during the high-temperature reduction has a profound effect on the distribution of deuteroethane.

The rate of HD formation in the D_2-H_2-ethene reaction is also plotted as a function of the catalyst reduction time in Figure 3.3. In contrast to the deuterated ethanes, the curve for HD formation decreased monotonously, but convex downward. The values of H/M (the number of chemisorbed hydrogen atoms divided by the number of metal atoms included in the catalysts) are also plotted against reduction time in Figure 3.3. The curve for HD formation is similar to that for the H/M value in its dependence on the reduction time.

Surface Reaction Sites Generated in the SMSI State

The degree of the migration of suboxide onto the metal surface in SMSI catalysts has been reported to be proportional to the square root of the reduction time. [5, 9] There should be three different reaction environments on the metal surface in the migration model for SMSI-metal/Nb_2O_5 systems, the bare metal surface (I), the perimeter of migrated NbO_x (II) and the NbO_x surface (III), as follows:

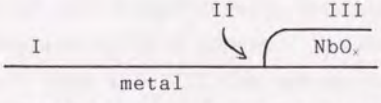

Assuming that NbO_x migrates onto the metal according to a diffusion process with self-similarity, the area of each environment can be written as a function of the high-temperature

reduction time (t_R) in the following equations:

site I (on metal) : $S_I(t_R) = S_0 - \alpha t_R^{1/2}$ (3.1)

site II (periphery): $S_{II}(t_R) = \beta t_R^{1/4}$ (3.2)

site III (on oxide) : $S_{III}(t_R) = \alpha t_R^{1/2}$ (3.3)

where α and β are the constants related with diffusion coefficient and $S_0 = S_I(0)$. The oxidation states of migrated Nb species have been suggested to be Nb^{2+}, Nb^{3+} or Nb^{4+}. [21] It is difficult, however, to characterize NbO_x at the metal surface precisely in the present systems. Nevertheless, the ethene hydrogenation activities of the Nb^{+} and Nb^{3+} species supported on SiO_2 or TiO_2 were negligible [22] under the present conditions, and the Nb^{5+} monomer [22] and Nb_2O_5 were inactive. It is likely that S_{III} does not contribute to the reaction.

The behavior of H/M, monotonous decreasing convex function, confirms the applicability of the (3.1) ~ (3.3) equations based on thermal diffusion process of NbO_x. And HD formation belongs to the same category, which suggests that deuterium adsorption step occurs on site I.

Site I and site II would retain the metallic nature so that the produced ethane would be smeared isotopically on both sites. The site for $d_0 > d_1 > d_2$ distribution should reflect the d_0-ethane formation most (in Figure 3.3) and it is to be site II because site I should be decreasing function as demonstrated in (3.1). Equations (3.1), (3.2) and (3.3) are coincident with (1.52), (1.53) and (1.51), respectively, and the discussion in chapter 1 can be applied to this system. Unfortunately, $[S_I][S_{II}]$ and $[S_{II}]^2$ (for site II) can not be distinguished one another in the combination with $[S_I]^2$ (for site I) because both combinations could give a maximum in t_R variation. But at least, for the reaction on site II, adsorption of hydrogen is not rate-

determining (In this case, r is proportional to $[S_I]^2$ and it never shows a maximum, assuming the number of site is overwhelming factor in the rate.) First hydrogen addition and interfacial reactions should be excluded from the rate-determining step because d_0-ethane is formed mainly at site II which is produce with isotopic dilution through hydrogen shuffling on site II. The most probable rate-determining step is, therefore, concluded to be I-2, i.e. hydrogen diffusion from site I to site II. This suggests that activation energy of this step agrees with that of deuterium adsorption or the contribution of this step did not appear in Arrhenius plot of HTR-Rh/Nb_2O_5 behind the formation on site I in Figure 3.1 due to small T^{-1} range.

The importance of peripheral site for the catalytic reaction has been reported also in CO hydrogenation. TiO_x/Rh foil has been demonstrated to show the maximum activity for methane formation in certain coverage of TiO_x. [23] It has not been clarified whether the kinetics including activation energy changed after decoration of TiO_x but this study support the different catalytic function of peripheral site proposed here.

Active Sites and Reaction Environments for Ethene Deuteration on SMSI Catalysts

While the static interaction of adsorbed species and surface structure has been extensively studied, there have been few studies which refer to the surface dynamic environments during catalysis, including the relationship between structures and isotopic concentrations at the surface. As already discussed, there are two characteristic sites in ethene deuteration on SMSI catalysts. On site I, the bare metal surface, D_2 dissociates and

ethene is associatively adsorbed, and on site II, the periphery of migrated NbO_x, only ethene is adsorbed to interact with deuterium/hydrogen atoms transported from site I. Under the conditions that D_2 dissociation and the diffusion are slow steps, the interconversion between associatively adsorbed ethene and half-hydrogenated species (and hence hydrogen exchange in ethene) readily occurs to dilute the deuterium on the surface. The surface isotopic ratio of deuterium concentration to hydrogen concentration may thus be different between site I and site II. The fact that d_0-ethane was the predominant product in the D_2-ethene reaction on site II in the SMSI catalyst indicates that the isotopic ratio (surface D/H) was significantly low at the NbO_x periphery. On the other hand, since d_2-ethane is main product on site I, the isotopic ratio (surface D/H) is considered to be large. In other words, the two sites are situated in different 'deuterium reserver' for site II in the SMSI state. A schematic model for ethene deuterogenation on Rh/Nb_2O_5 is illustrated in Figure 3.4. This model may also fit Ir/Nb_2O_5 because of the similar phenomena shown in Table 3.2 and 3.3. [24]

The catalytic activity is controlled by the hydrogen-dissociation process and diffusion, which is affected by both the number of sites and the electronic state of site I. There is no enhancement by SMSI for hydrogen dissociation on Rh/Nb_2O_5, while for Ir/Nb_2O_5 an enhancement was observed by a modification of the electronic state of the Ir metal, accompanied by a reduction in the activation energy. In contrast to the activity, the selectivity (relative population of deuteroethanes) is affected by the nature of site II at the perimeter of the NbO_x island.

There may be two kinds of effects which the NbO_x island

provides. One is a short-range effect which can exert an influence sat only one or two atom distances from the periphery, and the other is a long-range effect which causes an electronic modification of the metal surface. The importance of short-range influences by the hetero-adatom has been pointed out both experimentally [23] and theoretically [24, 25]. This influence may change the relative stability of the π- and di-σ-intermediates in the D_2-ethene reaction and suppress deuterium adsorption on metal atoms in the periphery of NbO_x. In contrast, the long-range effect may be weak, because no change in kinetic parameters was observed with LTR- and HTR-Rh/Nb_2O_5 under the present reaction conditions. For Ir/Nb_2O_5 it was positive for hydrogen or deuterium dissociation, since the energy barrier for dissociation was reduced. The difference between Rh and Ir in the enhancement of H_2-D_2 exchange and ethene hydrogenation in the SMSI state may be of interest. The phenomena observed on the Rh/Nb_2O_5 and Ir/Nb_2O_5 catalysts in the SMSI state may be more or less common to general metal catalysis with promoters.

References

1. B.Imerik, C.Naccache, G.Coudurier, H.Praliaud, P.Meriaudeau, G.A.Martin, J.C.Verdrine, *eds.*, "Metal-Support and Metal-Additive Effects in Catalysis", Elsevier, Amsterdam, 1982.
2. R.T.K.Baker, S.J.Tauster and J.A.Dumesic, "Strong Metal-Support Interactions", Am.Chem.Soc.Symp.Ser., **198**, American Chemical Society, Washington, DC., 1986.
3. D.E.Resasco, R.J.Fenoglio, M.P.Suarez and J.O.Cechini, *J.Phys.Chem.*, **90**, 4330 (1986).
4. P.Meriaudeuau, O.H.Ellestad, M.Dufaux and C.Naccache,

J.Catal., **75**, 243 (1983).

5. D.E.Resasco and G.L.Haller, *J.Catal.*, **82**, 279 (1983).
6. M.A.Vannice and R.L.Garten, *J.Catal.*, **56**, 236 (1979).
7. J.D.Bracy and K.Burch, *J.Catal.*, **78**, 389 (1984).
8. D.N.Benton, Y.M.Sun and J.M.White, *J.Am.Chem.Soc.*, **106**, 3059 (1984).
9. S.Takatani and Y.W.Chung, *J.Catal.*, **90**, 75 (1984).
10. H.R.Sadeghi and V.E.Hennrich, *J.Catal.*, **87**, 279 (1984).
11. J.Santos, J.Philips and J.A.Dumesic, *J.Catal.*, **81**, 147 (1983).
12. X.Z.Jiang, T.F.Hayden and J.A.Dumesic, *J.Catal.*, **83**, 168 (1983).
13. M.A.Vannice and C.Sudhakar, *J.Phys.Chem.*, **88**, 2429 (1984).
14. J.D.Bracy and R.Burch, *J.Catal.*, **86**, 384 (1984).
15. W.M.H.Sachtler, D.F.Shriver, W.B.Hollenberg and A.F.Long, *J.Catal.*, **82**, 429 (1985).
16. G.C.Bond, "Catalsis by Metals", Academic Press, London, 1962.
17. T.Keii, *J.Chem.Phys.*, **22**, 144 (1954).
18. C.Kemball, *J.Chem.Soc.*, 735 (1956).
19. G.C.Bond, J.J.Phillipson, P.B.Wells and J.M.Winterbottom, *Trans.Faraday Soc.*, **60**, 1847 (1960).
20. G.C.Bond, G.Webb, P.B.Wells and J.M.Winterbottom, *Trans.Faraday Soc.*, **61**, 1007 (1965).
21. B.A.Sexton, A.E.Hughes and K.Foger, *J.Catal.*, **77**, 85 (1977).
22. M.Nishimura, K.Asakura and Y.Iwasawa, *J.Chem.Soc., Chem.Commun.*, 1660 (1986); *Chem Lett.*, 573 (1987).
23. M.E.Levin, M.Salmeron, A.T.Bell and G.A.Somorjai, *J.Chem.Soc., Faraday Trans. 1*, **83**, 2061 (1987) ; M.E.Levin, M.Salmeron, A.T.Bell and G.A.Somorjai, *J.Catal.*, **106**, 401 (1987).

24. J.M.Maclaren, J.B.Pendry, R.W.Joyner and P.Meehan, *Surf.Sci.*, 175, 263 (1986).

25. J.M.Maclaren, J.B.Pendry and R.W.Joyner, *Surf.Sci.*, 178, 856 (1986).

Table 3.1 Estimation of average particle size (nm)

		H/M[a]	TEM	XRD
Rh/Nb_2O_5	LTR	10 (0.11)	9.8	9.3
	HTR	(0.01)	10.2	9.6
Ir/Nb_2O_5	LTR	4.0 (0.31)	4.2	4.2
	HTR	(0.00)	4.4	4.1

a: The particle sizes calculated from H/M values given in parentheses.

Table 3.2 Percentage distributions of deuteroethanes and gas-phase hydrogen formed in the initial stage of the D_2-ethene reaction on Rh/Nb_2O_5

	T/K	d_0	d_1	d_2	d_3	d_4	H_2[a]	HD[a]
LTR	210	30	28	42	0	0	0	2
	220	27	26	42	5	0	0	2
	233	11	23	60	5	1	1	3
HTR	213	51	8	41	0	0	0	0
	230	49	12	39	0	0	0	1
	253	48	15	37	0	0	0	1

The d_0 - d_4 distributions are the values at the extrapolation to 0 % conversion. a: Values at 5 % conversion in ethene deuterogenation. The residual percentage is due to D_2.

Table 3.3 Percentage distributions of deuteroethanes and gas-phasehydrogen formed in the initial stage of the D_2-ethene reaction on Ir/Nb_2O_5

	T/K	d_0	d_1	d_2	d_3	d_4	H_2 [a]	HD [a]
LTR	250	14	36	50	0	0	0	0
	263	19	33	48	0	0	0	0
	273	24	31	45	0	0	0	0
HTR	259	50	10	40	0	0	0	0
	273	46	8	46	0	0	0	0
	292	42	11	47	0	0	0	0

The d_0 - d_4 distributions are the values at the extrapolation to 0 % conversion. a: Values at 5 % conversion in ethene deuterogenation. The residual percentage is due to D_2.

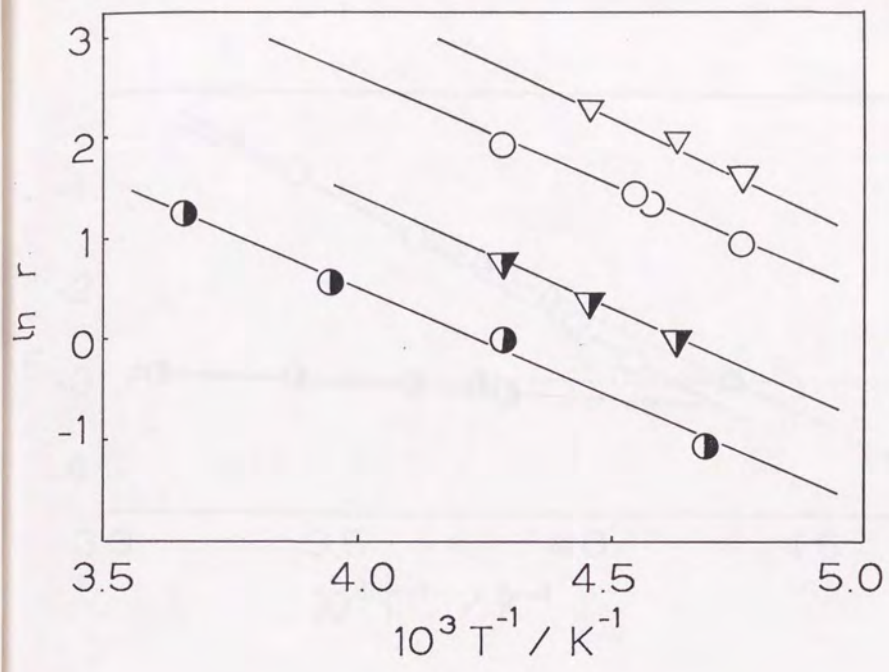

Figure 3.1 Arrehnius plots for ethane formation in the D_2-ethene reaction (P_{D_2} = $P_{CH_2=CH_2}$ = 1.1 kPa) and HD formation (P_{H_2} = P_{D_2} = 0.53 kPa and $P_{CH_2=CH_2}$ = 1.1 kPa) in the H_2-D_2-ethene reaction on Rh/Nb_2O_5 ; ◯ , ethane formation on the LTR catalyst; ▽ , HD formation on the LTR catalyst; ◑ ,ethane formation on the HTR catalyst; ▼ , HD formation on the HTR catalyst. The rates were normalized by the H/M value for the LTR catalyst.

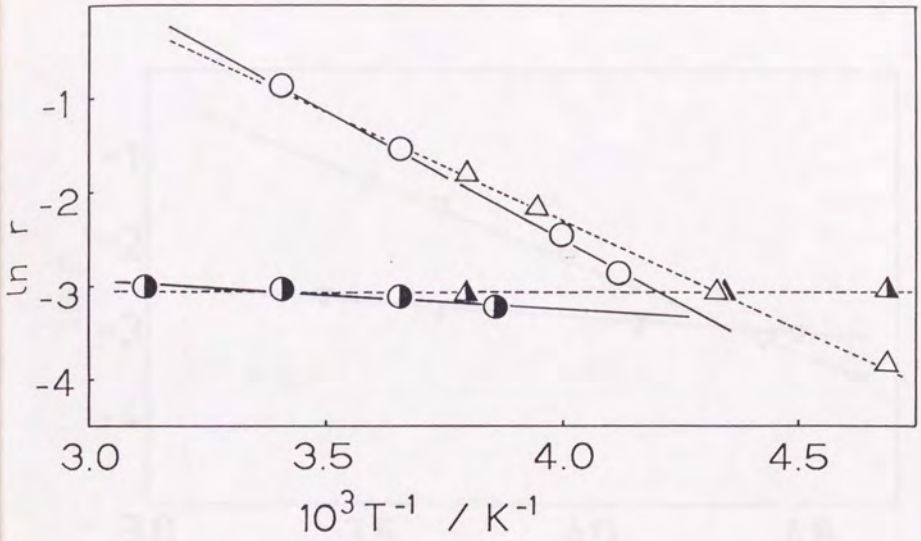

Figure 3.2 (a) Arrehnius plots for ethane formation in deutration and hydrogenation of ethene on Ir/Nb_2O_5 : ○ , D_2-ethene reaction on the LTR catalyst; ◑ , D_2-ethene reaction on the HTR catalyst; △ , H_2-ethene reaction on the LTR catalyst; ◭ , H_2-ethene reaction on the HTR catalyst. The rates are normalized by the H/M value for the LTR catalyst. $P_{D2} = P_{CH2=CH2} = 1.1$ kPa.

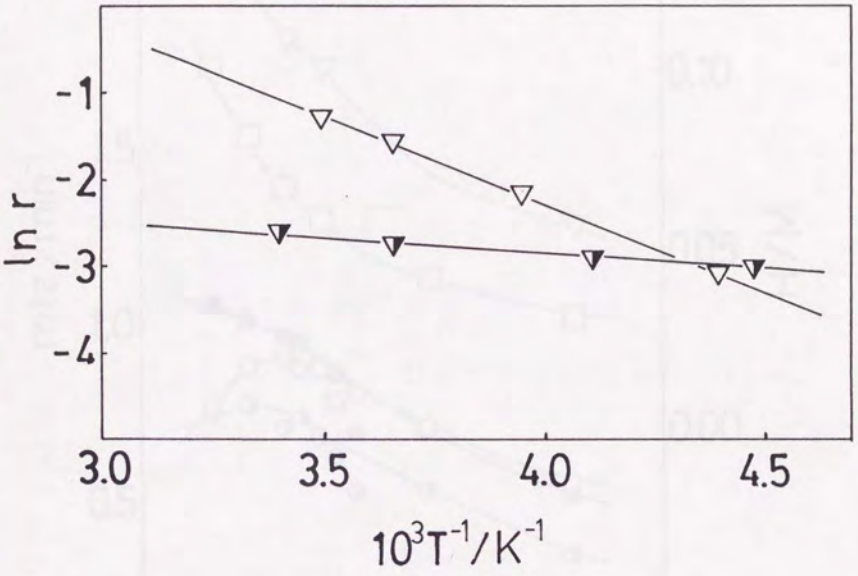

Figure 3.2 (b) Arrhenius plots for HD formation in the H_2-D_2-ethene reaction on Ir/Nb_2O_5 ; ▽ ,LTR; ▼ ,HTR. The rates are normalized by the H/M value for the LTR catalyst. $P_{H_2} = P_{D_2} =$ 0.53 kPa and $P_{CH_2=CH_2} = 1.1$ kPa.

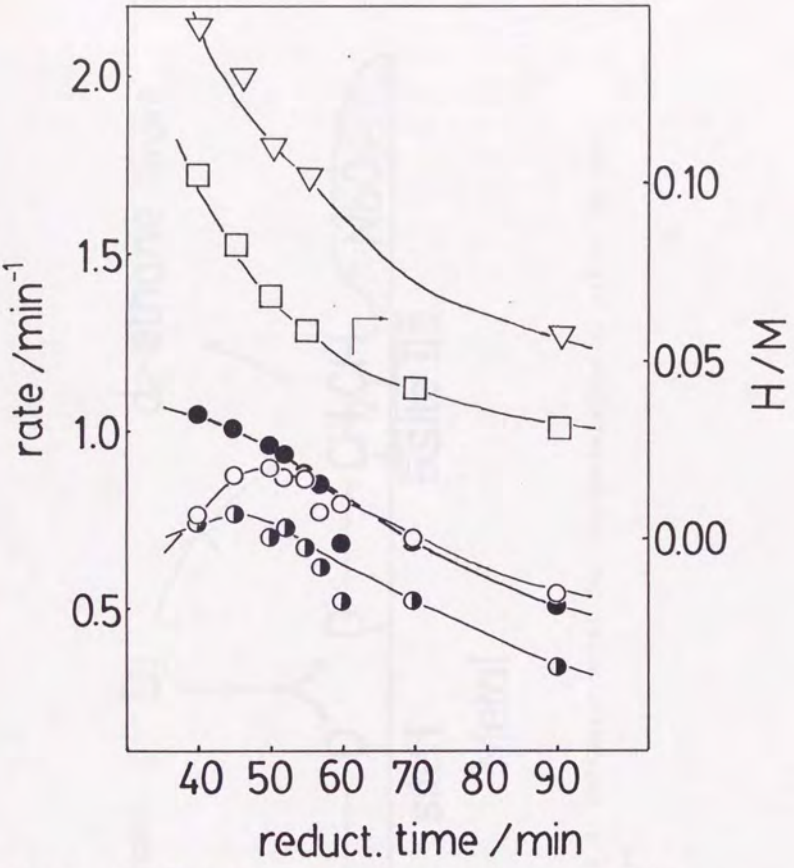

Figure 3.3 Reaction rates for each deuteroethane and HD formaiton on Rh/Nb_2O_5 and H/M values as a function of the high-temperature pretreatment (reduction) time of the catalyst: ○, d_0-ethane; ◑, d_1-ethane; ●, d_2-ethane; ▽, HD; □, H/M; reaction temperature, 216 K; catalyst reduction temperature, 673 K; $P_{D_2} = P_{CH_2=CH_2} = 1.1$ kPa for ethane formation, $P_{H_2} = P_{D_2} = 0.53$ kPa and $P_{CH_2=CH_2} = 1.1$ kPa for HD formation.

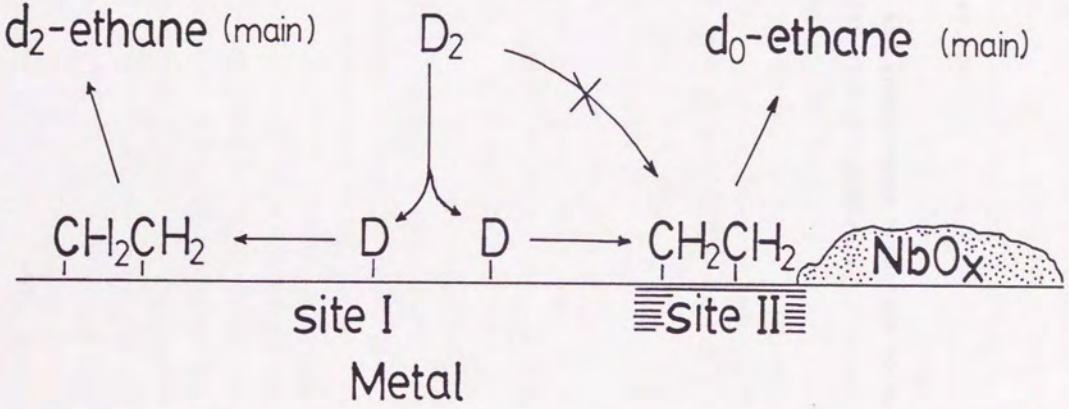

Figure 3.4 Schematic model for the deuteration of ethene on SMSI catalysts.

Chapter 4

Long- and Short-range Promotion by Sodium in D_2-CH_2=CH_2 Reaction over Pt Catalysts

The promoted catalysts have been reported to offer unique catalytic performance/phenomenon and unique microscopic reaction features induced by second elements. [1-3] Among them, alkali metals may result in a considerable modification of metal surface, due to the alternation of surface electronic structure by charge transfer. It has been demonstrated to reduce the strength of the adsorption of $CH_2=CH_2$ [4-6] and C_6H_6 [7] or to strengthen the adsorption of CO [8, 9] and NO [10]. The activation energy of CO hydrogenation decreases in the presence of alkali-metal, which is related to a large red shift of C-O stretching frequency. [11] In addition to the electronic modification of surface, several authors have pointed out short range effects of additives on adsorbates experimentally [12, 13] or theoretically [14, 15].

Metal catalysis is a dynamic process at the surface including short- and long-range interaction between adsorbates and additives. It is necessary for the microscopic clarification of alkali-metal additive effect in catalysis to investigate the reaction mechanism relating to surface structures reflecting the working state.

Chapter 3 demonstrated the local environments of reaction sites and the reaction mechanism of hydrogenations on SMSI catalysts, Rh/Nb_2O_5 and Ir/Nb_2O_5. On these SMSI catalysts the electronic modification of metal surfaces and the cooperative catalysis by two kinds of sites have been observed. In this chapter, the mechanism of D_2-ethene reaction on Na-promoted Pt/SiO_2 catalysts is presented in order to understand the microscopic surface states and the short- and long-range effects of Na additives in relation to the genesis of essential factors for catalysis of promoters.

4.1. Methods

SiO_2-supported platinum catalysts were prepared by a conventional impregnation method using aqueous solution of $H_2PtCl_6 \cdot 6H_2O$ (Soekawa Chemical Co.) or by co-impregnation with aqueous solution of Na_2CO_3 (Wako Pure Chemical Industries, 99.7 %) and $H_2PtCl_6 \cdot 6H_2O$. The impregnated samples were subsequently dried for 3 h at 393 K and calcined for 2 h at 773 K in air. Commercially available SiO_2 (Nippon Aerosil, ox-50, surface area: 50 $m^2 \cdot g^{-1}$) was used as a support. The loading of platinum was always 2.4 wt %. Five kinds of $Na/Pt/SiO_2$ catalysts were prepared with varying the amount of sodium; 0.19, 0.75, 1.5, 2.3, or 6.1 in atomic molar ratio, Na/Pt. The catalysts thus obtained were placed in a closed circulating system which can be evacuated below 10^{-4} Pa. Then they were treated with oxygen at 473 K for 1 h, followed by evacuation for 30 min, and reduced by hydrogen at 473 K for 1 h, followed by evacuation for 30 min before each catalytic reaction. These pretreatments can not expel the significant amount of sodium from silica surface. [16] Chlorine was not observed with all samples used by XPS in the wide scan mode. Hydrogen adsorption at 293 K was also carried out in this system.

In order to avoid a possible formation of $NaPtCl_6$ during the co-impregnation procedure, 2 step-impregnation method was also adopted for the preparation of a Na-promoted catalyst of Na/Pt = 1.5. SiO_2 was impregnated with aqueous Na_2CO_3 solution, Na-doped dried for 3 h at 393 K, and calcined for 2 h at 673 K in air. The Na-doped support thus obtained was again impregnated with aqueous solution of $H_2PtCl_6 \cdot 6H_2O$. The following procedure was

similar to that for coimpregnation samples. Resultant $Pt/Na \cdot SiO_2$ catalyst gave the same results in the experiments, such as H/M, TEM and D_2-CH_2=CH_2 reaction, as those for $Na/Pt/SiO_2$ with Na/Pt = 1.5.

The particle size of platinum metal in the catalysts was determined by transmission electron microscope (TEM). The electronic states of elements and surface composition in the catalysts were examined by XPS (Shimadzu, ESCA 750). The absence of chlorine, sulfur and the other poisoning elements was confirmed in wide scan mode.

Ethene (Takachiho Trading Co., 99.9%) was further purified by freeze-thaw cycles before each catalytic reaction. Hydrogen and deuterium gases of research grade were purified through a 5A molecular-sieve trap at 77 K.

The products of reactions were analyzed by gas chromatograph with a TCD or by mass spectrometer operating with 70 eV electrons after the separation by a 2 m VZ-10 column at 343 K.

The adsorbates on the catalysts were observed by IR (JASCO FT/IR-7000 with 2 cm^{-1} resolution). The catalysts were molded into self-supporting disks and mounted in the cell which can be heated to 773 K. The IR cell was combined in a closed circulating system mentioned above.

4.2. Results and Discussion

(i) The structure and electronic state of the catalyst surface.

The average particle size estimated by TEM and the dispersion determined by hydrogen adsorption (H/M) are summarized in Table 4.1. The dispersion decreased with an increase of Na

content, which is comparable with the increase in the particle size. However, the dispersion expected from the particle size of TEM [17] was smaller than H/M in the presence of Na, assuming that one H atom corresponded to one surface Pt atom and Pt particles are spherical. The comparison of Pt dispersion evaluated by two different experiments would be valid to some extent because both values of dispersion from H/M and TEM are almost the same in the unpromoted catalyst. Since hydrogen is not adsorbed on sodium at room temperature, the surface ratio of Na to Pt, coverage θ_{Na}, can be evaluated from the difference in the dispersion calculated by H_2 adsorption and TEM. The results of the estimation are listed in the last column of Table 4.1.

The degree of error in the dispersion calculated from TEM should be described because the size of the Pt particles on the SiO_2 (ox-50) are usually distributed, involving smaller and larger particles. The Pt particle sizes were distributed relatively uniformly as illustrated in TEM photographs of Figure 4.1. The deviation from the average particle size is estimated to be ± 1.2 nm. Accordingly, the error of Na coverage in Table 1 was evaluated to be ± 0.1. Nevertheless, it is to be noted that the values of Na coverage are the averaged values for Pt particles contained in each catalyst.

The particle size was enlarged by Na addition (4.1 nm to 8.0 nm)in spite of the similar preparation conditions. It did not essentially depend on the amount of Na through in the range $0.75 \leq Na/Pt \leq 6.1$. The surface coverage θ_{Na} was constant to be 0.2. Therefore, it is likely that the Na/Pt particles are stable when the diameter is around 8 nm. Pt particles in the catalyst with Na/Pt = 0.16 is thought to be in a mixed state of Pt particles with and without Na.

Table 4.2 shows the results of XP spectra, in which the binding energies of Pt $4f^{7}/_{2}$ and Na 1s are listed. The binding energy of Pt decreased by the loading of Na and continuously decreased with an increase of Na quantity. Since the particle size was almost the same in the range of more than Na/ Pt = 0.75, the shift of the binding energy may result from the electron donation from Na to Pt rather than extra-atomic relaxation or particle size effect. The binding energy ranging from 1073.4 eV to 1073.8 eV of Na 1s suggests that the state of Na is Na^{+} as Na_2O [18]. The peak intensities of Pt (I_{Pt}) and Na (I_{Na}) as a function of Na loading are plotted in Figure 4.2 where I_{Pt} was normalized by H/M due to surface area calibration. I_{Pt} was constant in Na/Pt $\geq$ 0.75, which is consistent to the constant coverage of Na on Pt particle in Table 4.1. I_{Pt} for Na/Pt = 0.19 was similar to I_{Pt} for the samples with Na/Pt $\geq$ 0.75. This may indicate that Na cluster/particles with a similar size start to cover the Pt particle surfaces from a low content of Na.

On the other hand, I_{Na} increased monotonously, showing an upward curvature. It suggests that Na is also loaded on SiO_2 support. Moreover, I_{Na} profile in Figure 4.2 shows a saturation curve. In contrast to Na on Pt particles, the Na on SiO_2 surface is suggested to grow to form the larger islands by increasing Na loading. The most probable growth mode of $Na/Pt/SiO_2$ catalyst surface as a function of the Na amount is illustrated in Figure 4.3.

(ii) Effects of Na additives on Hydrogenation Rate and Activation Energy.

The activities and activation energies of ethene deuteration

are listed in Table 4.3. In the presence of sodium, the rate of ethane formation became about 4 times higher as compared with that on the unpromoted catalyst. The activation energy (41 $kJ \cdot mol^{-1}$) was a little higher than that of Pt/SiO_2 catalyst(33 $kJ \cdot mol^{-1}$). As for $Na/Pt/SiO_2$, the rate increased with an increase of the sodium loading, while the activation energy was kept constant. It is known that the rate-determining step of ethene hydrogenation on group VIII metals at lower temperatures is hydrogen dissociation and the apparent activation energy is positive. At higher temperatures the rate-determining step shifts to the second-hydrogen addition and the apparent activation energy is often negative. [19] In the case of $Na/Pt/SiO_2$, the reaction temperatures are low enough (208 K - 312 K) and the activation energies are positive. And the partial pressure dependence of the rate was well fitted to the equation:

$$r = k_{D_2} \times P_{D_2} / (1 + K_E \times P_E)$$

where P_{D_2} and P_E are the partial pressures of deuterium and ethene, respectively. k_{D_2} and K_E are constants. This rate equation implies a relatively strong adsorption of ethene and the rate-determining deuterium dissociation. This is confirmed by the fact that the rate data for ethene deuteration and hydrogen exchange had almost equal Arrhenius parameters as shown in Table 4.3. The rate of HD formation in H_2-D_2 exchange reaction on Pt/SiO_2 under the deuteration conditions was much larger than the rate of ethane formation. Furthermore, the activation energy for HD formation on Pt/SiO_2 (19 $kJ \cdot mol^{-1}$) was smaller than that for ethane formation (33 $kJ \cdot mol^{-1}$). This difference suggests that there is a kind of site on Pt/SiO_2 which is active mainly for H_2-

D_2 exchange reaction on Pt/SiO_2. In other words, there may be at least two kinds of sites --- one is active only for deuterium dissociation, where HD formation preferentially proceeds, and the other is the site on which deuterium and ethene react by the above equation. On $Na/Pt/SiO_2$, two kinds of sites with the different character do not exist because the activation energies and the preexponential factors were almost equal for ethane and HD formations. One reasonable explanation is the blockage of HD site by Na.

The Pt particle size and the Na coverage remained in the range of Na/Pt from 0.75 to 6.1, but ethane formation was enhanced by increasing Na loading. The extent of charge transfer from Na to platinum is roughly estimated from the shift of the binding energy of Pt $4f_{7/2}$ of $Na/Pt/SiO_2$. The more negative the charge of platinum was, the more rapidly the ethane formation proceeded. The electron transfer from sodium to platinum on SiO_2 surface is ascribed to a direct interaction between them and an indirect interaction through the support.

A break was observed at ca. 250 K in the Arrhenius plot for $Na/Pt/SiO_2$ (Na/Pt = 0.19). The activation energy in the lower temperature region was 32 $kJ \cdot mol^{-1}$ and in the higher temperature region was 40 $kJ \cdot mol^{-1}$. These values are similar to those for Pt/SiO_2 and $Na/Pt/SiO_2$ ($Na/Pt \geq 0.75$), respectively. This result for $Na/Pt/SiO_2$ (Na/Pt = 0.19) also indicates a mixed state of the Pt particles with and without Na as illustrated in Figure 4.3.

Ethene hydrogenation has been regarded as structure insensitive in usual. In fact, there was no large difference between two Pt/SiO_2 catalysts with different dispersions, H/M = 0.67 and 0.014 in the hydrogenation. The rate of ethene formation per surface Pt atom on the H/M = 0.014 catalyst was more than 80

% of that for the catalyst with H/M = 0.67. The activation energy was also unchanged. It is unlikely that the enhancement of these parameters by Na addition comes from the particle size enlargement.

(iii) Isotope distributions in the products

Table 4.4 summarizes the percentage distributions of d_i-ethane ($i=1,2,\cdots,6$) at the initial stage of ethene deuteration on the catalysts with various Na loading. The amount of deuterium atom incorporated in ethane molecule ($\Sigma id_i/6\Sigma d_i$) are also listed in Table 4.4. $\Sigma id_i/6\Sigma d_i$ increased from 0.31 to 0.38 in the presence of Na, whereas it was almost independent of the amount of Na. The increase of $\Sigma id_i/6\Sigma d_i$ for the promoted catalyst may be referred to the following two possible causes; the adsorption of deuterium increased comparing to ethene and/or the equilibrium between associatively adsorbed ethene and half-hydrogenated intermediates shifted, these change leading to the change of H/D ratio at the surface.

Chapter 3 demonstrated for SMSI catalysts that there are site I (bare metal site) and site II (periphery site) and H/D ratios at the surface are different between these sites. On these surfaces with two different sites d_i-ethane should be produced in the order, d_0, $d_2 > d_1$ on whole surface. It was illustrated that ethene isotopes were produced on site I or site II alone in the order, $d_2 > d_1 > d_0$ or $d_0 > d_1 > d_2$, respectively. In the case of Na-promoted Pt/SiO_2 catalysts, the order is $d_2 > d_1 > d_0$ and there is no evidence of the H/D heterogeneity for ethane formation.

(iv) Active sites and intermediates for hydrogenation and hydrogen exchange

The rates of ethene deuteration and hydrogen exchange in D_2 + $CH_2=CH_2$ system as a function of Na loading are shown in Figure 4.4. The products in the hydrogen exchange reaction were d_1-ethene (C_2H_3D) and d_2-ethene ($C_2H_2D_2$). d_3- and d_4-ethene were negligible and below the detection limit in the initial stage of the reaction. The exchange rate is defined as an amount of deuterium atom in d_i-ethene (Σid_i) produced per unit time, while the deuteration rate is the sum of the formation rate of deuterated ethanes. The deuteration rate increased with an increase of the amount of Na while the exchange rate was almost constant except Na/Pt = 0.00. Thus the rate of ethane formation seems to have a correlation with the binding energy of Pt $4f^7/_2$, while the rate of exchange reaction correlates with the Na coverage on Pt surface. These results suggest that deuteroethene is formed at the neighboring sites of Na_2O island (periphery site) and ethane is produced at the far sites (bare metal sites). The theoretical works has demonstrated that the electronic modification should be large at the periphery sites which might be located in the region of two or three atoms around Na because of the screening of platinum metal. [15]

The XP spectra for Pt $4f^7/_2$ could not distinguish the periphery sites from bare metal sites. It may be because the ratio of the periphery sites should be less than that of the bare metal sites considering the small coverage of Na (0.2) and the particle size is large enough.

Figure 4.5 shows IR spectra of adsorbed ethene in the C-H stretching region. Both adsorption and measurement were carried

out at 293 K. Five peaks were observed for each catalysts in Figure 4.5. Three higher-wavenumber peaks, 3078 cm^{-1}, 3025 cm^{-1} and 2965 cm^{-1} for Pt/SiO_2 and 3078~9 cm^{-1}, 3025 cm^{-1} and 2964 cm^{-1} for $Na/Pt/SiO_2$ are due to π-ethene. The largest peaks at 2888~2869 cm^{-1} are assigned to di-σ-ethene on Pt. [20] The absorption band in 2803 cm^{-1} on Pt/SiO_2 has been attributed to the first overtone of the asymmetric CH_3 bending mode of ethylidyne. [20] These peaks diminished rapidly when D_2 was added at 293 K, evolving deuterated ethenes and ethanes in gas phase. This can result from that the observed surface species are the reaction intermediates for ethane formation and ethene-deuterium exchange. The position and relative intensity of the peaks for π-ethene were not affected by sodium addition. On the contrary, the band for di-σ-ethene shifted by 18 cm^{-1} (Na/Pt = 0.19) ~ 24 cm^{-1} (Na/Pt = 6.1) and the relative intensity to those of π-ethene became smaller comparing to that for Pt/SiO_2. A small peak for di-σ-ethene was observed for the catalyst of Na/Pt = 0.19 (2889 cm^{-1}), the position being the same as that for Pt/SiO_2. This supports the mixed state of pure Pt and Na-containing Pt particles in $Na/Pt/SiO_2$ (Na/Pt = 0.19) as mentioned above.

The peak positions of π-ethene (around 2965 cm^{-1}) and for di-σ-ethene are plotted against the Na loading in Figure 4.6. The ratio of the intensity of these two bands (I_π/I_σ) was also plotted as a function of Na loading in Figure 4.6. The ratio, I_π/I_σ, for $Na/Pt/SiO_2$ was much larger than that for Pt/SiO_2 and was almost independent of the Na loading. These results suggest that the π-ethene is located at the periphery sites, while the di-σ-ethene is formed on the bare sites as demonstrated in Figure 4.7.

The constant peak position of π-ethene shows that the change in the electronic state characterized by Pt $4f_{7/2}$ XP spectra does not influence the electronic state of π-ethene, more precisely, C-H stretching. On the other hand, the C-H stretching of di-σ-ethene changed still after the saturation coverage of Na at 0.20, due to the further electronic effect from sodium supported on SiO_2 surface.

From the above discussion the most probable mechanism is deduced; ethane is preferentially formed at the bare metal sites through the di-σ-intermediate, while ethene-deuterium exchange mainly proceeds at the periphery sites through the π-intermediate. The ratio of di-σ-ethene/π-ethene adsorbed on $Na/Pt/SiO_2$ decreased as compared with that on Pt/SiO_2 and the C-H stretching frequency shifted toward lower wavenumber. The electronic effect on the Pt surface is reflected in the increase of the activation energy for ethane formation. However, the rate of ethane formation increased with the Na-promoted Pt/SiO_2 catalysts due to the less adsorption of di-σ-ethene to lead to the enhancement of hydrogen dissociation which competitively takes place as suggested by the rate equation. The C-H peak position of π-ethene and the rate of the ethene-deuterium exchange at the periphery sites were almost independent of the Na quantity. These results indicate the constant size of the Na_2O on Pt particles over the whole range of Na loading.

References

1. B.Imelik, C.Naccache, G.Condurier, H.Praliaud, P.Meriaudeau, P.Gallezot, G.A.Martin, J.C.Vedrine, ed. "Metal-Support and Metal-Additive Effects in Catalysis", Elsevier, Amsterdam,

1982.

2. S.J.Thomson, *J.Chem.Soc., Faraday Trans. 1*, **83**, 1893 (1987).
3. J.H.Sinfelt, "Bimetallic Catalysts", John Wiley & Sons, 1984.
4. X.L.Zhou, X.Y.Zhu, J.M.White, *Surf.Sci.*, **193**, 387 (1988).
5. R.G.Windham, M.E.Bartram, B.E.Koel, *J.Phys.Chem.*, **92**, 2862 (1988).
6. R.G.Windham, B.E.Koel, *J.Phys.Chem.*, **94**, 1489 (1990).
7. E.L.Garfunkel, J.J.Maj, J.C.Frost, M.H.Farias, G.A.Somorjai, *J.Phys.Chem.*, **87**, 3629 (1983).
8. J.E.Crowell, E.L.Garfunkel, G.A.Somorjai, *Surf.Sci.*, **121**, 303 (1982).
9. E.L.Garfunkel, J.E.Crowell, G.A.Somorjai, *J.Phys.Chem.*, **86**, 310 (1982).
10. M.Kishinova, G.Pirug, H.P.Bonzel, *Surf.Sci.*, **140**, 1 (1984).
11. S.Kesraoui, R.Oukaci, D.G.Blackmond, *J.Catal.*, **105**, 432 (1987).
12. L.Ng, K.J.Uram, Z.Xu, P.L.Jones, J.T.Yates,Jr., *J.Phys.Chem.*, **86**, 6523 (1987).
13. M.E.Levin, M.Salmeron, A.T.Bell, G.A.Somorjai, *J.Chem.Soc., Faraday Trans.1*, **83**, 2061 (1987).
14. J.M.MacLaren, D.D.Vvedensky, J.B.Pendry, R.W.Joyner, *J.Chem. Soc., Faraday Trans 1*, **83**, 1945 (1987).
15. R.W.Joyner, J.B.Pendry, D.K.Saldin, S.R.Tennison, *Surf.Sci.*, **95**, 1(1984); J.M.MacLaren, J.B.Pendry, R.W.Joyner, P.Meehan, *Surf.Sci.*, **175**, 263 (1986).
16. V.Perrichon, M.C.Durupty, *Appl.Catal.*, **42**, 217 (1988).
17. R.Anderson, "Structure of Metallic Catalysts", P.361, Academic Press, New York, 1975.
18. H.Onishi, C.Egawa, T.Aruga, Y.Iwasawa, *Surf.Sci.*, **191**, 479 (1987).

19. G.C.Bond, "Catalysis by Metals", Academic Press, London, 1962.

20. S.B.Mohsin, M.Trenary, H.J.Robota, *J.Phys.Chem.*, **92**, 5229 (1988).

Table 4.1 Dispersion and particle size of platinum in the catalysts.

Na/Pt	H/M	TEM(/nm)[a]	Na coverage[b]
0.00	0.31	4.1 (0.30)	0
0.19	0.24	5.5 (0.22)	0.1
0.75	0.13	8.0 (0.16)	0.2
1.5	0.13	8.0 (0.16)	0.2
2.3	0.13	7.8 (0.17)	0.2
6.1	0.13	7.9 (0.16)	0.2

a: the values in the parentheses are the estimated dispersion by TEM after Anderson. [17], b: calculated from the results of H/M and TEM.

Table 4.2 The binding energies of peak top in $Pt4f^{7}/_{2}$ and Na 1s in XP spectra of the catalysts.

Na/Pt	$Pt4f^{7}/_{2}$ (eV)	Na 1s (eV)
0.00	70.53	
0.19	70.38	1073.4
0.75	70.28	1073.4
1.5	70.14	1073.5
2.3	70.08	1073.7
6.1	70.02	1073.8

Table 4.3 Activities(r) and activation energies (E) of ethene deuteration and exchange on the catalysts with different sodium loading.

Na/Pt	ethane[a]		HD[b]	
	E/kJ·mol^{-1}	r	E/kJ·mol^{-1}	r
0.00	33	1.00	19	4.03
0.19	40[c]	1.22		
0.75	41	3.20	40	3.07
1.5	41	3.31	40	3.35
2.3	41	3.53	41	3.56
6.1	41	3.98	40	4.10

a: $D_2 + CH_2=CH_2$ reaction at 273 K (P_{D_2} = 1.3 kPa, $P_{CH_2=CH_2}$ = 3.0 kPa), b: $D_2 + H_2 + CH_2=CH_2$ reaction at 273 K($P_{D_2} = P_{H_2}$ = 0.6 kPa, $P_{CH_2=CH_2}$: 3.0 kPa), c: T ≥ 250 K.

Table 4.4 The percentage distribution of d-ethane at the initial stage of D_2 + $CH_2=CH_2$ reaction at 263K[a].

	Na/Pt					
ethane	0.0	0.19	0.75	1.5	2.3	6.1
d_0	10	8	7	9	10	13
d_1	24	15	19	19	16	15
d_2	45	38	34	36	37	36
d_3	13	21	21	20	18	15
d_4	8	18	19	13	12	12
d_5	0	0	0	3	7	9
d_6	0	0	0	0	0	0
$100\Sigma id_i/6\Sigma d_i$	31	38	38	36	38	38

a: $P_{D2} = P_{CH2=CH2} = 1.3$ kPa.

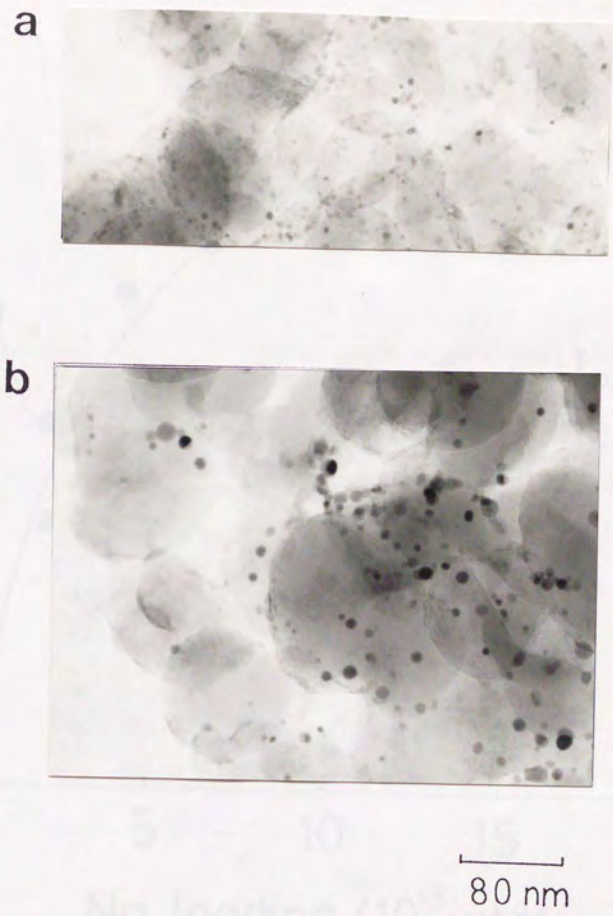

Figure 4.1 TEM photographs of the catalysts. a: Pt/SiO_2 (Na/Pt = 0.00), b: $Na/Pt/SiO_2$ (Na/Pt = 1.5)

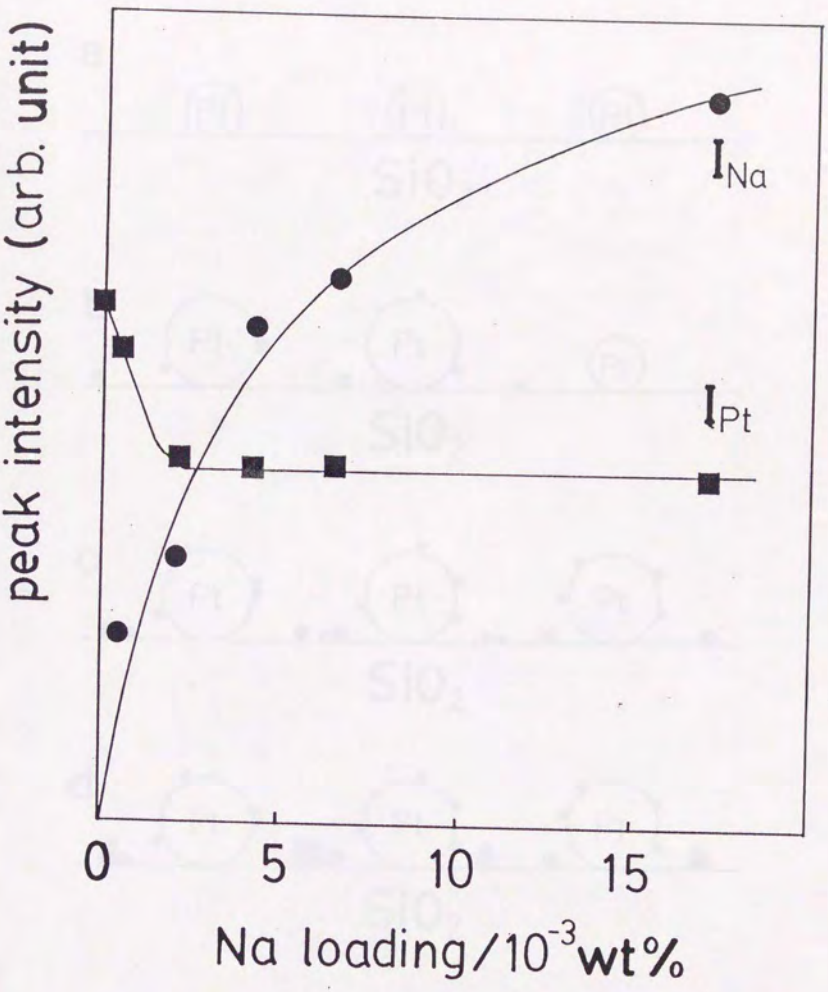

Figure 4.2 Peak intensities of Pt $4f^{7}/_{2}$ and Na 1s as a function of Na loading. Each peak was integrated and normalized by that of Si 2p of the sample. Pt $4f^{7}/_{2}$ was corrected by H/M to avoid the decrease of surface area due to enlarging of particle size and to deduce the coverage of Na.

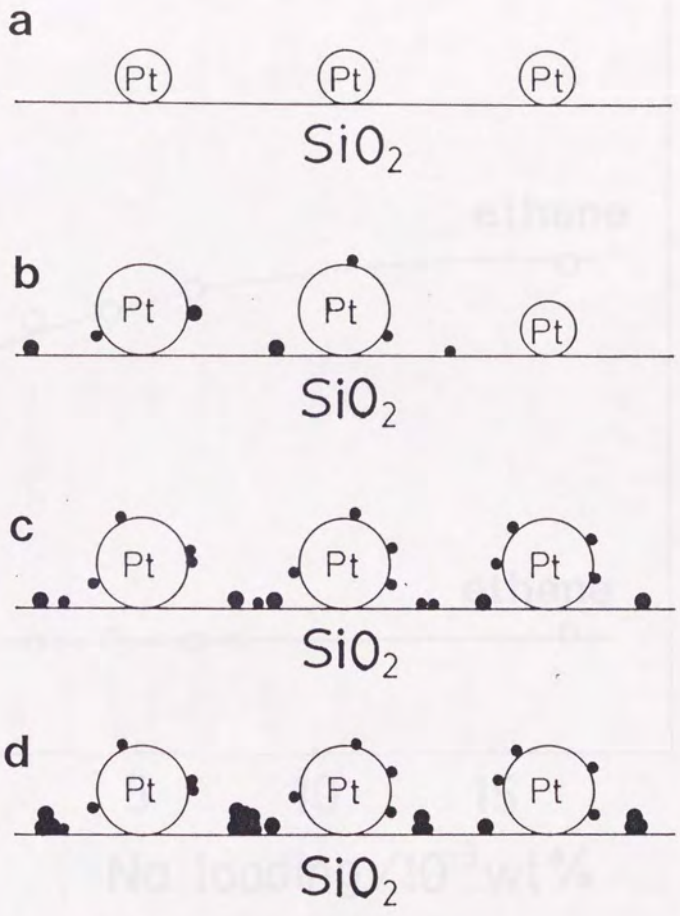

Figure 4.3 Schematic models for $Na/Pt/SiO_2$ with various Na loading. a: Na/Pt = 0.00, b: Na/Pt = 0.25, c: Na/Pt = 1.0, d: Na/Pt = 4.0.

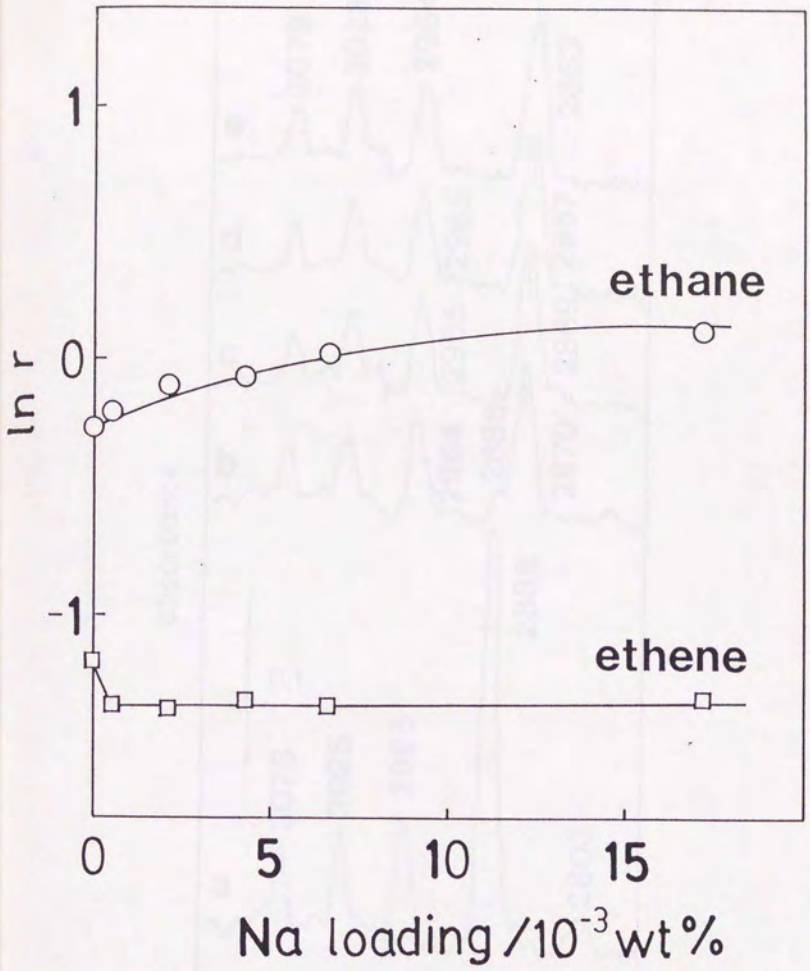

Figure 4.4 The initial rates for ethane formation and ethene exchange. P_{D_2} = 1.3 kPa, $P_{CH_2=CH_2}$ = 5.0 kPa, the reaction temperature = 250 K.

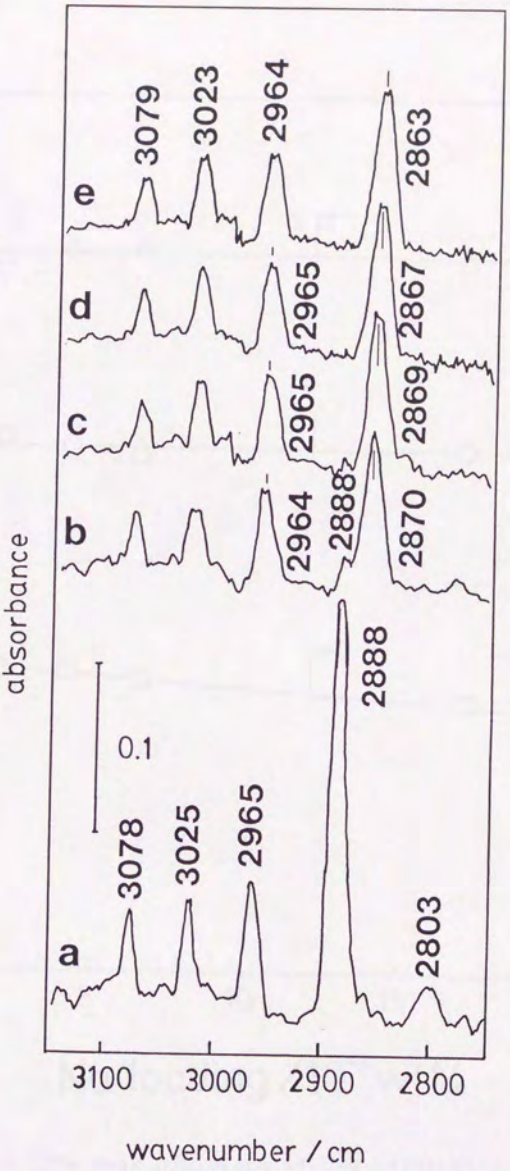

Figure 4.5 IR spectra of C-H stretching region for ethene adsorbed on Na/Pt/SiO_2 catalysts; a: Na/Pt = 0.00 (Pt/SiO_2), b: Na/Pt = 0.19, c: Na/Pt = 0.75, d: Na/Pt = 1.5, e: Na/Pt = 6.1.

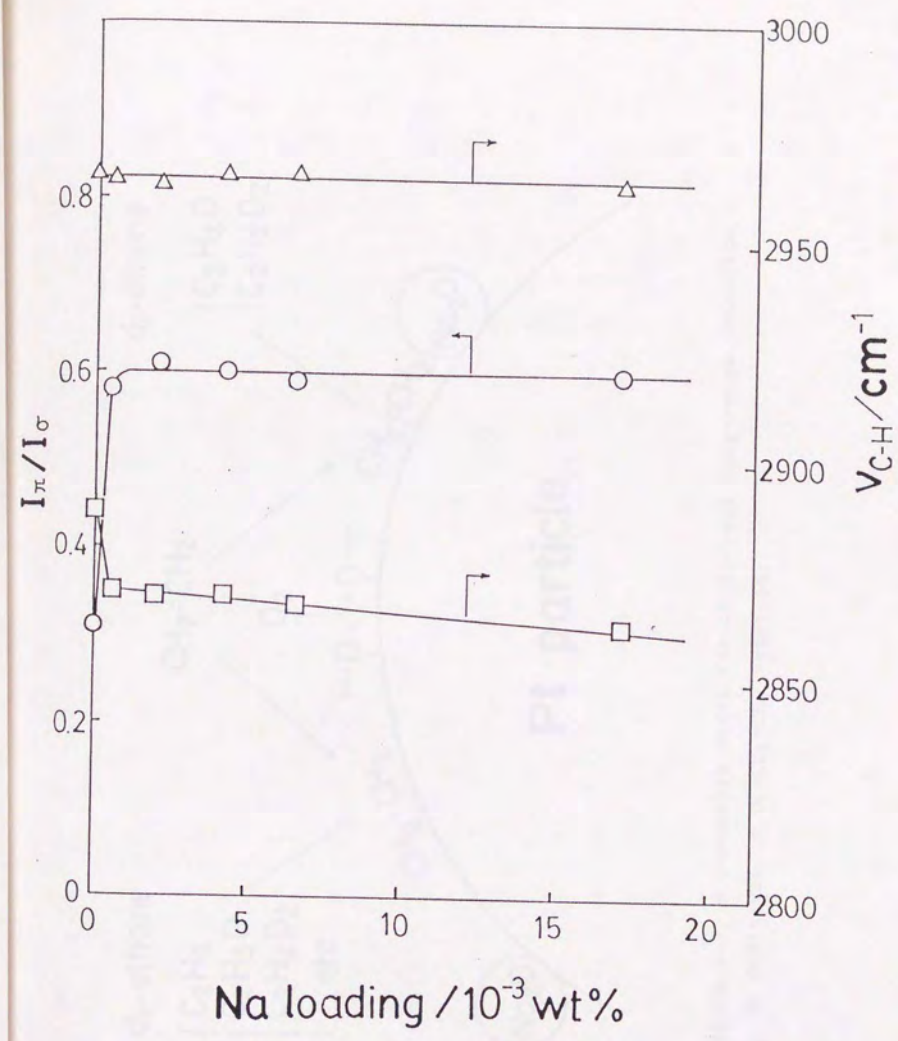

Figure 4.6 The peak positions of C-H stretching for π-ethene (△) and di-σ-ethene (□) and the ratio of these peak intensities (I_π/I_σ , ○) as a function of Na loading.

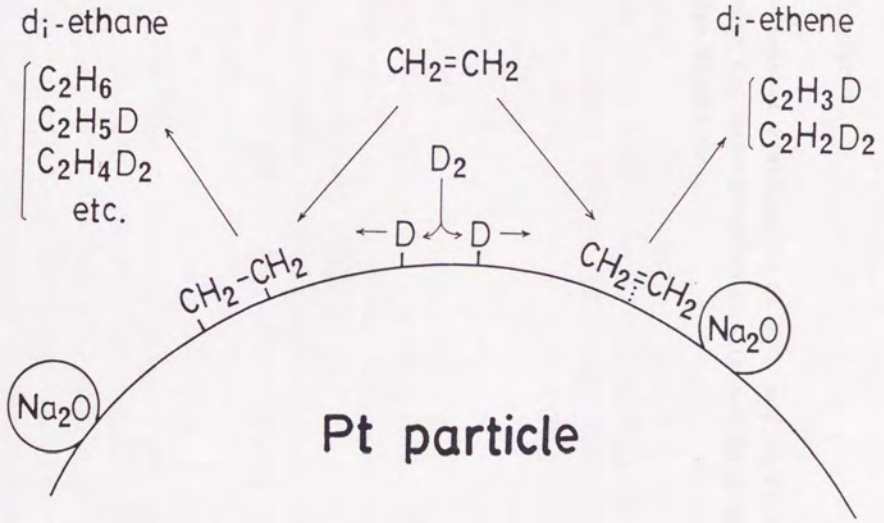

Figure 4.7 A schematic model for short- and long-range promotion by Na additives in $D_2+CH_2=CH_2$ reaction.

Chapter 5

d-State of Platinum in Pt/SiO_2 and $Na/Pt/SiO_2$ Catalysts under C=C Hydrogenation Conditions by X-ray Absorption Near-edge Structure

The promoting effects of supports or additives on the catalysis of group VIII metals have been demonstrated to be based on many factors, but the electronic modification of metals may be one of indispensable and universal aspects brought by promoters. Thus the electronic properties of the metal ensembles are often key ingredients for the elucidation of the genesis or the mechanism of noble-metal catalysis. The change in the density of d-electrons should be most essential for metal catalysis since the adsorption or activation of reactants arises mainly from the interaction of d-electrons with frontier orbitals of reactant molecules.

The white lines emerging at X-ray adsorption edges of platinum correspond to the electronic transition from 2p core electrons to unoccupied 5d-state of Pt by photon absorption. The L_2 edge arises from the $2p_{1/2}$ states and L_3 edge arises from the $2p_{3/2}$ states. It has been clarified that the intensity of the white lines well reflects the electronic characteristics of platinum catalyst and this relation has been applied to the supported catalysts under vacuum [1-4] or ambient oxygen, hydrogen or carbon monoxide. [5-7] Further, the degree of unoccupied d-states of Pt has quantitatively been estimated by the intensity of the white lines [8] in investigating metal-support interactions [9-11].

It has been reported that catalytic reactions are sometimes originated from the change of the structures and electronic states of metal sites, which is hardly pictured from static experiments. [12-14] Thus *in-situ* studies of the working catalyst are desirable. This chapter intends to describe the relation between the elementary steps and the electronic state of the metal catalysts with monitoring the density of unoccupied d-

states of supported Pt catalysts under C=C hydrogenation condition. Molecule-molecule interaction through the metal often plays an important role at the key step of the reaction to change the rate or the selectivity. The introduction of substituents to C=C compounds in this study should belong to this level. And the electron donation by the metal-additives which composes the catalyst surface could be also affective to the catalysis. Both two levels are promotion effect as Thomson pointed out. [15] For both cases the measurement of d-state of platinum is monitoring the media of electron between molecule and molecule or molecule and alkali metal in a working state of the catalyst.

5.1 Methods

The catalysts were prepared with the same methods in chapter 4.

XANES (X-ray absorption near-edge structure) spectra were measured in the transmission mode at BL-7C of Photon Factory, National Laboratory for High Energy Physics (KEK-PF; proposal No. 89-007). The samples were prepared in a closed circulating system and transferred to in-situ X-ray absorption cell.

$CH_2=CH_2$, $CH_2=CHCH_3$ (Takachiho Trading Co.,Ltd., 99.9%), $CH_2=CHCN$, $CH_2=CHCOCH_3$ (Tokyo Kasei Co.,Ltd.) and $CH_2=CHCF_3$ (Japan Halon, 99.9%) were purified by freeze-thaw cycles before use. Deuterium (Takachiho Trading Co.,Ltd. research grade) was purified through a 5A molecular-sieve trap at 77 K. $D_2+CH_2=CHX$ (X = H, CH_3, CN, $COCH_3$, CF_3) reactions were carried out in the closed circulating system mentioned above and the products were analyzed by gas chromatograph using VZ-10 or PEG-1500 columns. No side-reaction other than deuterium/hydrogen addition was

observed. No catalytic reaction proceeds in the absence of deuterium or hydrogen.

Data analyses of the white lines at $L_{2,3}$ edges were performed in a similar way to that reported by Mansour et al.[8], *i.e.* comparison of the total unoccupied d-density of the sample (h_T) to that of the reference (Pt foil; h_r) at L_2 and L_3 edges as follows:

$$h_T = (1.0 + f_3)h_r \tag{5.1}$$

$$f_3 = (\Delta A_3 + 1.11\Delta A_2)/(A_{3,r} + 1.11A_{2,r}) \tag{5.2}$$

$$\Delta A_3 = A_3 - A_{3,r}, \quad \Delta A_2 = A_2 - A_{2,r} \tag{5.3}$$

where

A_3 : Intensity of L_3 edge absorption of the sample
A_2 : Intensity of L_2 edge absorption of the sample
$A_{3,r}$: Intensity of L_3 edge absorption of the reference
$A_{2,r}$: Intensity of L_2 edge absorption of the reference

The value of h_r has been reported to be 0.30. [16] The spectral area of the white line from the edge position to the next local minimum in the XANES spectrum was integrated and normalized by the edge jump to give the intensities of A_2, A_3, $A_{2,r}$ or $A_{3,r}$.

5.2 Results

Arrhenius plots for CH_2=CHX (X = H, CH_3, CN, $COCH_3$, CF_3) deuteration on 2.4 wt%-Pt/SiO_2 are shown in Figure 5.1. The

slopes are similar for all alkenes and the activation energy derived from them is 33 kJ·mol^{-1}. The relative rates decreased in the order, $-CF_3$ > $-CH_3$ > -H > $-COCH_3$ > -CN. The order is usually explained quantitatively by Hammett's parameter σ_P of the substituents as plotted in Figure 5.2, which exhibits a linearity with all the substituents except for $-CF_3$; the following equation is fitted;

$$\ln r = -6.4\ \sigma_P + 1.4 \qquad \text{(except } -CF_3\text{)} \qquad (5.4)$$

The typical XANES spectra of Pt L_3 edge of Pt/SiO_2 in the presence of CH_2=CHX (X = H, CH_3, CN, $COCH_3$, CF_3) are illustrated in Figure 5.3. The value of f_d derived from the XANES spectra are listed in Table 5.1, together with σ_P. The electron withdrawing character of total adsorbed molecules can be estimated by the difference (Δf_d) between f_d(CH_2=CHX)-f_d(none), which is also listed in Table 5.1. f_d was observed to correlate with σ_P except for CH_2=$CHCF_3$. As for CH_2=$CHCF_3$, f_d was much smaller than expected from σ_P, which may be related to its extremely high reaction rate in Figure 5.2.

f_d for Pt in $Na/Pt/SiO_2$ under vacuum as a function of Na loading is plotted as circles in Figure 5.4. The figure clearly shows that the density of unoccupied d-state of Pt decreases with an increase of Na quantity.

The particle size of Pt was enlarged in the presence of Na, as demonstrated in chapter 4, *i.e.*, the dispersion of Pt particles measured by hydrogen adsorption was 0.31 for Pt/SiO_2 and 0.13 for $Na/Pt/SiO_2$ with Na/Pt = 0.75 ~ 6.1. The density of unoccupied d-state has been demonstrated to depend on the particle size of Pt in Pt/SiO_2 catalyst. [1, 2] Table 5.2 shows

the variation of f_d and h_1 with the particle size of Pt/SiO_2. d-Electron density decreased with the particle size but the difference is a little for $H/M < 0.3$. Thus it is concluded that the effect of the particle size on the value of f_d is little as $H/M \leq 0.30$ for the present $Na/Pt/SiO_2$ catalysts. Hence the change of f_d in Figure 5.4 is ascribed mainly to the electron donation from sodium to platinum.

The kinetic parameters for the reaction and the amounts of molecule adsorbed on the catalysts are summarized in Table 5.3. The rates (r) of ethane formation on $Na/Pt/SiO_2$ under identical conditions were plotted against the Na quantity in Figure 4.4. r increased in accordance with Na loading. The reaction was promoted by the addition of Na as demonstrated in chapter 4. And the rate was expressed by the following equation:

$$r = k_{D_2} P_{D_2} / (1 + K_E P_E) \qquad (5.5)$$

where P_{D_2} and P_E are the partial pressures of D_2 and ethene, respectively, and k_{D_2} and K_E are constants. This equation is the same as in chapter 4. The values in Table 5.3 were obtained through the least square fitting to equation 5.5. The activation energies were a little changed from 33 $kJ \cdot mol^{-1}$ for Pt/SiO_2 to 41 $kJ \cdot mol^{-1}$ for $Na/Pt/SiO_2$, but they were independent of Na loading. The adsorption amount of ethene was measured at certain intervals during the reaction to give θ_{C_2}, the coverage of ethene, by the extrapolation to the value at the initiation of the reaction. The coverage also decreased according as the Na amount.

In order to examine the relationship of catalytic performance with the electron density of d-state, f_d was measured

in the presence of ethene similarly to catalytic reaction conditions. The values are plotted as filled circles in Figure 5.4 where f_d is illustrated as a function of Na amount contained in the catalysts. f_d was once decreased and increased with the Na loading in contrast to under vacuum. This is the effect of total ethene adsorbed on the Pt surface.

5.3 Discussion

(i) The linear energy relationship and Pt d-state density

The linear free energy relationship (LFER) has been found in many chemical reactions of organic compounds. One of the indicators widely used is Hammett's σ. LFER has been reported in the dissociation reaction of olefin ligands in mononuclear organometallic complexes, $L_nM-\!\!\parallel\!\!\diagdown_{X}^{\diagup} \rightleftarrows L_nM + \!\!\diagup\!\!=\!\!\diagdown_{X}$. [17-19] According to these studies, a negative correlation between σ_P and the dissociation constant (K_d) was generally observed. It suggests that the strength of the chemical bond between C=C and group 8 metal is mainly controlled by the π-backdonation from d-state (virtual HOMO) of the metal to LUMO of the ligand. All the CH_2=CHX compounds used in the present paper have been proved to show the LFER without any exception in $Ni(P(o\text{-tolyl})_3)_2$ system, [17] in which K_d becomes smaller as σ_P of X is larger. Thus, it is suggested that the adsorption of CH_2=CHX on Pt becomes strong with the larger σ_P and the deuteration rate should be damped, because the rate or ethene deuteration is represented by equation 5.5 which is based on the competitive adsorption of D_2 and CH_2=CH_2 and the rate determining adsorption of D_2. In this context, several questions arise; (1) was LFER really valid

for heterogeneous hydrogenation systems? (2) does the d-state of Pt change during the reaction? and (3) does the change in the d-state affect the reaction mechanism for ethane formation? How about the activation energy, and the frequency factor?

For the rate of the deuteration, an LFER is shown in Figure 5.2. This is consistent to the rate expression 5.5. Consequently, it is rationalized to monitor the d-state under the reaction conditions in the presence of CH_2=CHX. The density of unoccupied d-state of Pt in Pt/SiO_2 changed in relation to the electron-withdrawing character of substituents (X) of CH_2=CHX (σ_P) except for X = CF_3 as demonstrated in Table 5.1. The larger σ_P of the substituent, the larger the unoccupied d-state becomes. Nevertheless, this d-electronic change brought no electronic modification to the step of D_2 adsorption as rate-determining step. In fact, Figure 5.1 showed the same activation energy for all CH_2=CHX. The rate variation with the kind of CH_2=CHX results from the alternation of the preexponential factor in the rate constant(k_{D_2}).

The rate for the deuteration of CH_2=$CHCF_3$ is much larger than that expected from the line in LFER of Figure 5.2. A small change in d-density, Δf_d, observed on the adsorption of CH_2=$CHCF_3$ in Table 5.1 demonstrates a weak adsorption of the molecule on platinum. It has been reported that the mode of adsorption on Pt(111) and (100) is not dissociative, [20, 21] excluding the contribution of self-hydrogenation to alkane formation and the direct interaction between fluorine and platinum. In fact, no formation of $CH_3CH_2CF_3$ by CH_2=$CHCF_3$ alone was observed with Pt/SiO_2 catalyst and no hydrogenolysis was observed under the reaction condition. σ_P has been demonstrated to have a good correlation with the associative constant in

mononuclear complexes. [17] On the other hand, CH_2=CHX adsorbs on multi-metal sites at Pt(111) and (100) surfaces. [20, 21] σ_I may not always reflect the strength of electron-withdrawing character of substituents (X) at metal surfaces. The effective value of σ_I for $-CF_3$ on Pt surface is evaluated to be -0.28 from Figure 5.2.

(ii) The donation by Na_2O and the distribution of electron during the reaction.

Another way to modify the interaction between C=C bond and Pt is to add alkali-metal to the surface. The electron withdrawing group makes LUMO of CH_2=CHX low and the electron-donating additive makes the Fermi level high. These may strengthen the chemical bond between C=C bond and Pt to result in the suppression of D_2 adsorption.

The behavior of f_d in Figure 5.4 is explained by electron donation from Na_2O added, which fills the unoccupied d-state of Pt as a function of the amount of Na. This is consistent to Pt $4f_{7/2}$ in X-ray photoemission spectroscopy (XPS) of chapter 4 where the binding energy shift as a function of Na amount was observed.

The unoccupied d-state of Pt in $Na/Pt/SiO_2$ varied from 0.32 (Na/Pt = 0.0) to 0.22 (Na/Pt = 6.1) in Figure 5.4. The values of h_f for Pt/SiO_2 in Table 5.2 varied from 0.35 to 0.31 with different particle sizes and h_f for 0.7%-Pt/SiO_2 prepared by ion exchange method was reported to be 0.37. [9] Thus the change in h_f by Na addition is comparable to that by particle size, but the values for small Pt particles are larger than h_f (= 0.30), whereas the Na additives make the value smaller than h_f.

An increase of the activity for ethane formation (Figure 4.4) and the continuous decrease of K_E (Table 5.3) indicate that the filling d-states suppresses the adsorption of $CH_2=CH_2$. The adsorption of ethene on Pt single crystal has been suggested to be weakened by alkali metal in the literature. [22, 23] The decrease of k_{D_2} by the small amount of Na may be due to the increase of activation energy and the site-blocking of Na_2O on Pt surface. In contrast to K_E, k_{D_2} increased with an increase of Na quantity in Table 5.3, while the activation energy was kept constant. These results show that the adsorption of ethene on platinum in a working state of $D_2+CH_2=CH_2$ reaction is suppressed when the density of d-state under vacuum becomes larger by Na and, as a result, the rate of D_2 dissociation is increased. This may be contradictory to the HOMO-LUMO interaction picture [24] for the adsorption as discussed above. Then, it is natural to have the questions about the density of d-state of Pt and the strength of the adsorption of ethene in a working state of the catalyst.

The number of electrons in d-state extracted per adsorbed ethene increased linearly up to 0.76 at Na/Pt = 6.1 as already seen in Figure 5.5. But most of the charge gained by Pt were found to be lost under ambient $CH_2=CH_2$ gas, that is, extra charge from Na_2O is almost extracted by ethene adsorbed on Pt. Little change of the density of unoccupied d-state under reaction conditions can claim almost no change in the activation energy in Table 5.3. Thus it is suggested that ethene molecules play a role of electron buffer at Pt surface during the deuteration of ethene on $Na/Pt/SiO_2$ by means of the increase not of the number of adsorbed ethene but of the number of electron accepted by one ethene molecule adsorbed. Filled circles of Figure 5.4

illustrates the whole state of platinum particles which is proper to discuss the electronic effect on D_2 adsorption, but does not show the microscopic state around active sites and adsorbed ethene. Thus f_d in Figure 5.4 was converted into the amount of electron extracted per a molecule.

As shown in Figure 4.6 in chapter 4, the acceptor of electron is di-σ-ethene in the system of $Na/Pt/SiO_2$ adsorbing $CH_2=CH_2$. And it was demonstrated that the reaction intermediate for ethane formation in $D_2+CH_2=CH_2$ reaction on $Na/Pt/SiO_2$ catalyst is di-σ-ethene, while that for hydrogen-exchange during the reaction is π-ethene. The former reaction occurs on the far-site on Pt surface and the latter on the neighbor site around Na_2O. No IR band shift implies π-species remains in the same environment in the presence of Na_2O. π- and di-σ-ethenes are main adsorbates as intermediates on the noble metals at room temperature. [25] The ratio, di-σ/(π + di-σ), on $Na/Pt/SiO_2$ was estimated to be 0.7 by the analysis of deuterated ethane and ethene produced by the reaction of the two kinds of adsorbates with D_2. The degree of electrons eliminated per di-σ-ethene ($\Delta h_{T^{\circ}_{d}}$) is shown in Figure 5.5, assuming that no π-ethene accept the extra charge of Pt. The maximum value of $\Delta h_{T^{\circ}_{d}}$ is 1.1 (Na/Pt = 6.1) and it is suggested that the adsorbed intermediate for ethane formation on $Na/Pt/SiO_2$ is di-σ-CH_2-$CH_2$$^{n-}$ where n varies from 0.1 to 1.1. The electron buffer, therefore, would work on $Na/Pt/SiO_2$ by means of the increase not of the number of adsorbed ethene but of the number of electron accepted by one ethene molecule adsorbed. Thus the initial sharp drop of f_d by Na addition (Figure 5.4) is attributed to the decrease of surface Pt atoms (increase of the particle size) in the presence of Na.

5.4 Summary

1. In the adsorption of CH_2=CHX (X: H, CH_3, $COCH_3$, CF_3, CN) on Pt/SiO_2 catalyst, f_d of Pt was correlated with the Hammett's σ_p of X except CF_3, *i.e.*, the higher the σ_p, the larger the density of unoccupied d-state is.
2. The reaction rates for the deuterogenation of CH_2=CHX including CH_2=$CHCF_3$ were inversely correlated with the density of unoccupied d-state determined from the white lines in XANES spectra at Pt L_2 and L_3 edges.
3. The addition of Na_2O to Pt/SiO_2 increased the activation energy a little, bur promoted ethene deuterogenation as a function of Na quantity.
4. The promotion of the rate is due to the decrease of the amount of adsorbed ethene and hence due to the increase of the preexponential factor of the rate constant for D_2 dissociative adsorption which is rate-determining.
5. The Na_2O additives decreased the unoccupied d-state density of Pt under vacuum. Na donates electron to d-band of Pt.
6. However, under the reaction conditions, most of the electrons of the d-state donated from Na_2O moved to ethene adsorbate.
7. The number of d-electrons abstracted per an adsorbed ethene molecule was proportional to the Na quantity in $Na/Pt/SiO_2$ catalysts.
8. The acceptor of the electrons was suggested to be di-σ-ethene which is reaction intermediate for ethene formation.

References

1. P.H.Lewis, *J.Phys.Chem.* **67**, 2151 (1963).

2. J.A.Horsley, F.W.Lytle, *ACS Symp.Ser.*, Amer.Chem.Soc., Washington D.C., **298**, 10 (1986).
3. F.W.Lytle, *J.Catal.* **43**, 376 (1976).
4. P.Gallezot, R.Weber, R.A.Dalla Betta, M.Boudart, *Z.Naturforsch.* **34a**, 40 (1979).
5. F.W.Lytle, P.S.P.Wei, R.B.Greegor, G.H.Via, J.H.Sinfelt, *J.Chem.Phys.* **70**, 4849 (1979).
6. T.Fukushima, J.R.Katzer, D.E.Sayers, J.Cook, *10th int.Congr. Cat.* 1988, vol.1, p.79.
7. B.J.McHugh, G.Larsen, G.L.Haller, to be published.
8. A.N.Mansour, J.W.Cook,Jr., D.E.Sayers, *J.Phys.Chem.* **88**, 330 (1984).
9. D.R.Short, A.N.Mansour, J.W.Cook,Jr., D.E.Sayers, J.R.Katzer, *J.Catal.* **82**, 299 (1983).
10. A.N.Mansour, J.W.Cook,Jr., D.E.Sayers, R.J.Emrich, J.R.Katzer, *J.Catal.* **89**, 462 (1984).
11. D.E.Resasco, R.S.Weber, S.Sakellson, M.McMillan, G.L.Haller, *J.Phys.Chem.* **92**, 189 (1988).
12. Y.Iwasawa, K.Asakura, H.Ishii, H.Kuroda, *Z.Phys.Chem.*, **144**, 105 (1985).
13. K.Asakura, Y.Iwasawa, *J.Phys.Chem.* **93**, 4213 (1989).
14. K.Asakura, K.K.Bando, K.Isobe, H.Arakawa, Y.Iwasawa, *J.Am.Chem.Soc.*, **112**, 3242 (1990).
15. S.J.Thomson, *J.Chem.Soc., Faraday Trans.1*, **83**, 1893 (1987).
16. M.Brown, R.E.Peierls, E.A.Stern, *Phys.Rev.B* **15**, 738 (1977).
17. C.A.Tolman, *J.Am.Chem.Soc.* **96**, 2780 (1974).
18. T.Yamamoto, A.Yamamoto, S.Ikeda, *J.Am.Chem.Soc.* **93**, 3360 (1971).
19. R.Cramer, *J.Am.Chem.Soc.* **86**, 217 (1964).
20. T.A.Clarke, I.D.Gay, B.Law, R.Mason, *Faraday Discuss.Chem.*

Soc. **60**, 119 (1976).

21. T.A.Clarke, I.D.Gay, R.Mason, *Chem.Phys.Lett.* **4**, 562 (1974).
22. R.G.Windham, B.E.Koel, *J.Phys.Chem.* **92**, 2862 (1988).
23. X.L.Zhou, X.Y.Zhu, J.M.White, *Surf.Sci.* **193**, 387 (1988).
24. I.Fleming, *Frontier Orbitals and Organic Chemical Reactions*, John Wiley & Sons: London, 1976; Chapter 2.
25. N.Sheppard, *Ann.Rev.Phys.Chem.* **39**, 589 (1988).

Table 5.1 f_d for 2.4%-Pt/SiO_2 under 1.3 kPa of CH_2=CHX.

CH_2=CHX	σ_P	f_d	Δf_d *
none		0.058	
CH_2=$CHCH_3$	-0.17	0.076	0.018
CH_2=CH_2	0.00	0.133	0.075
CH_2=$CHCOCH_3$	0.50	0.190	0.132
CH_2=$CHCF_3$	0.54	0.074	0.016
CH_2=CHCN	0.66	0.212	0.154

*Δf_d = f_d (CH_2=CHX) - f_d (none).

Table 5.2 The dependence of f_d and h_T on the particle size in Pt/SiO_2.

loading	H/M	f_d	h_T
0.9%	0.67	0.17	0.35
2.4%	0.31	0.06	0.32
4.7%	0.014	0.02	0.31

Table 5.3 The kinetic parameters for ethane formation and the amount of adsorbates during the reaction.

Na/Pt	E_a /kJ·mol^{-1}	K_E /Pa^{-1}	k_{D2} /Pa^{-1}·min^{-1}	θ_{C2}
0.00	33	1.8 * 10^{-3}	2.3 * 10^{-2}	0.94
0.75	41	8.8 * 10^{-4}	1.7 * 10^{-3}	0.87
1.5	41	8.2 * 10^{-4}	1.8 * 10^{-3}	0.86
2.3	41	7.6 * 10^{-4}	3.8 * 10^{-3}	0.83
6.1	41	6.8 * 10^{-4}	7.5 * 10^{-3}	0.71

E_a : activation energy, the same as in chapter 4. K_E and k_{D2} : constants in the rate expression $r = k_{D2} P_{D2} / (1+K_E P_E)$. θ_{C2} : the converage of adsorbed ethene during the reaction, which is normalized by the number of the surface Pt atoms measured by hydrogen adsorption experiment. Reactions were carried out at 247 K and the base pressure of the reactants is 1.3 kPa.

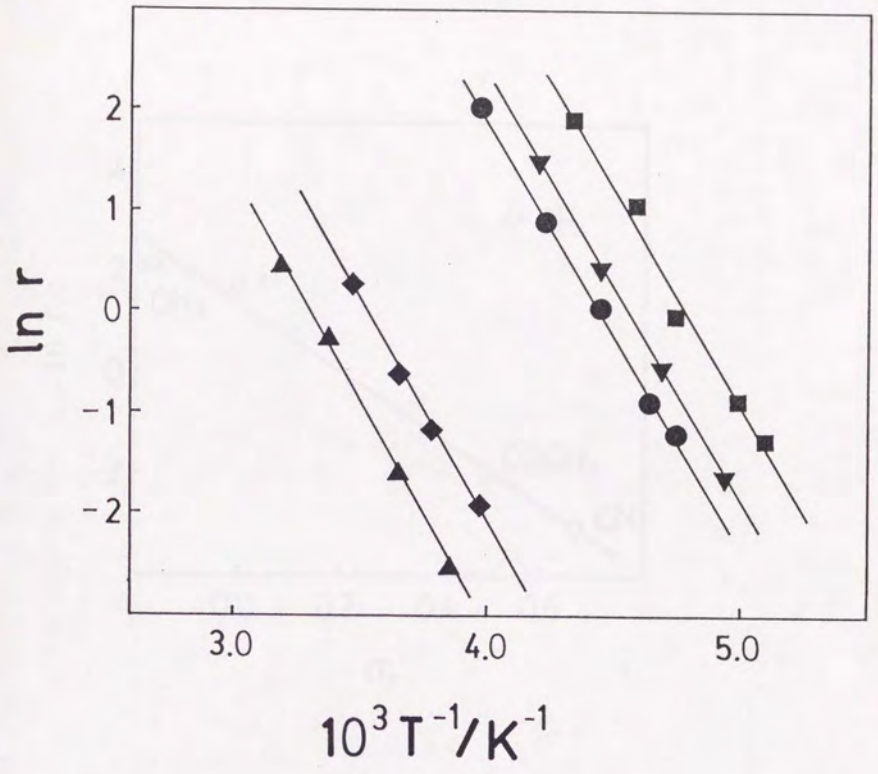

Figure 5.1 Arrhenius plots for CH_2=CHX deuteration.

■ : CH_2=$CHCF_3$, ▼ : CH_2=$CHCH_3$, ● : CH_2=CH_2,

◆ : CH_2=$CHCOCH_3$, ▲ : CH_2=CHCN.; $P_{CH_2=CHX}$ = P_{D_2} = 1.3 kPa.

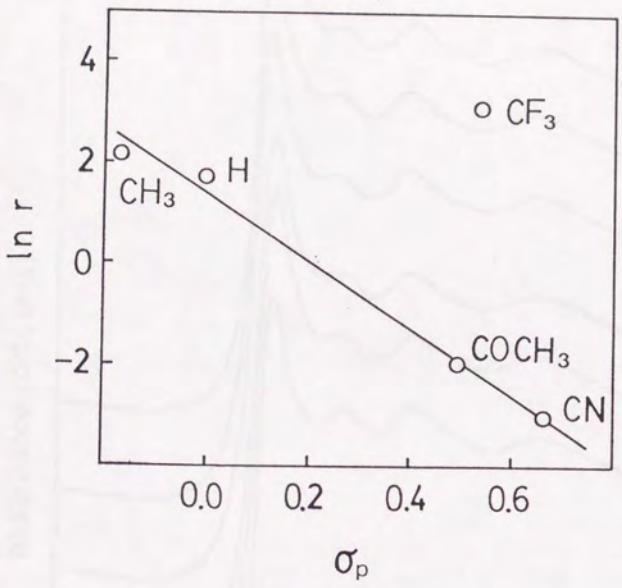

Figure 5.2 Linear free energy relationship between σ_p and reaction rate at 273 K. The reactions were carried out at $P_{CH_2=CHX} = P_{D_2} = 1.3$ kPa.

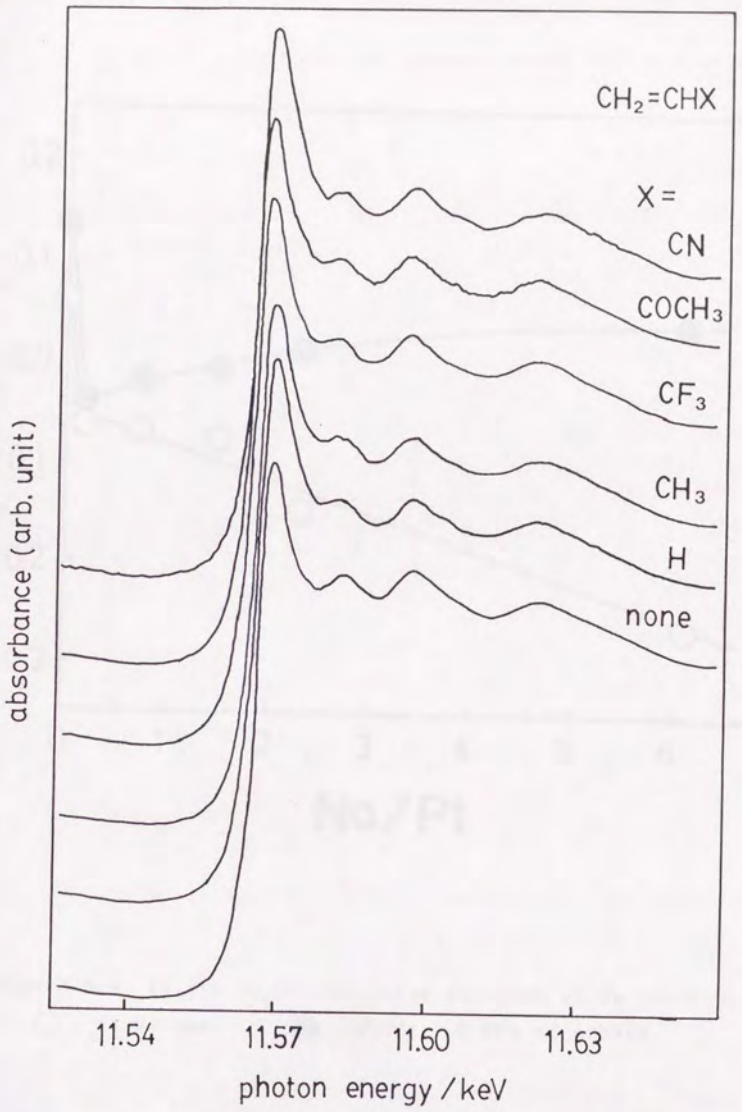

Figure 5.3 XANES spectra at Pt L_3 edges for Pt/SiO_2 under $P_{CH_2=CHX}$ = 1.3 kPa.

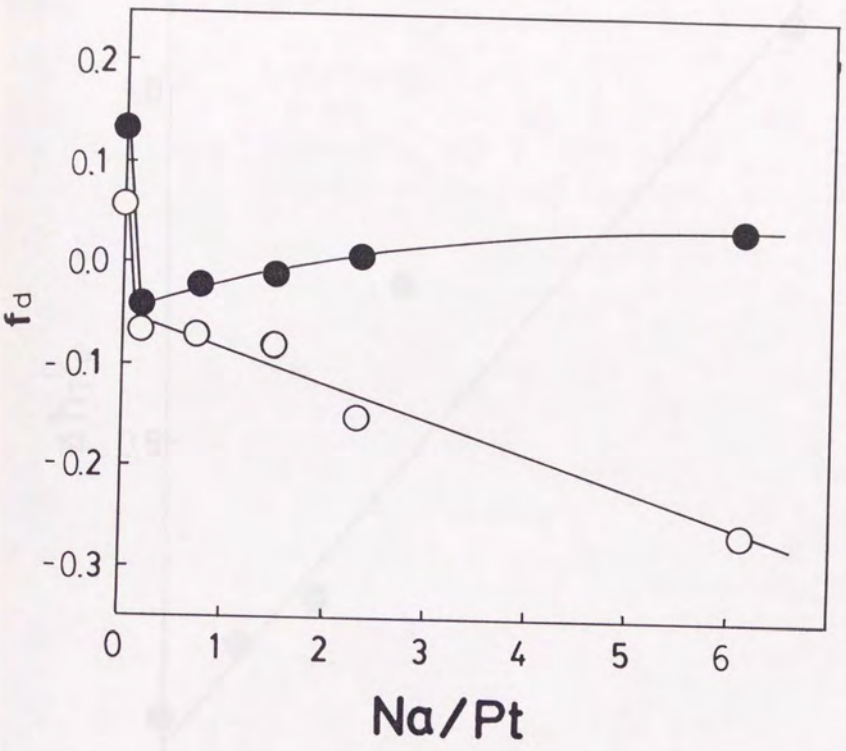

Figure 5.4 f_d for $Na/Pt/SiO_2$ as a function of Na loading.
○ : in vacuum, ● : under 1.5 kPa of ethene.

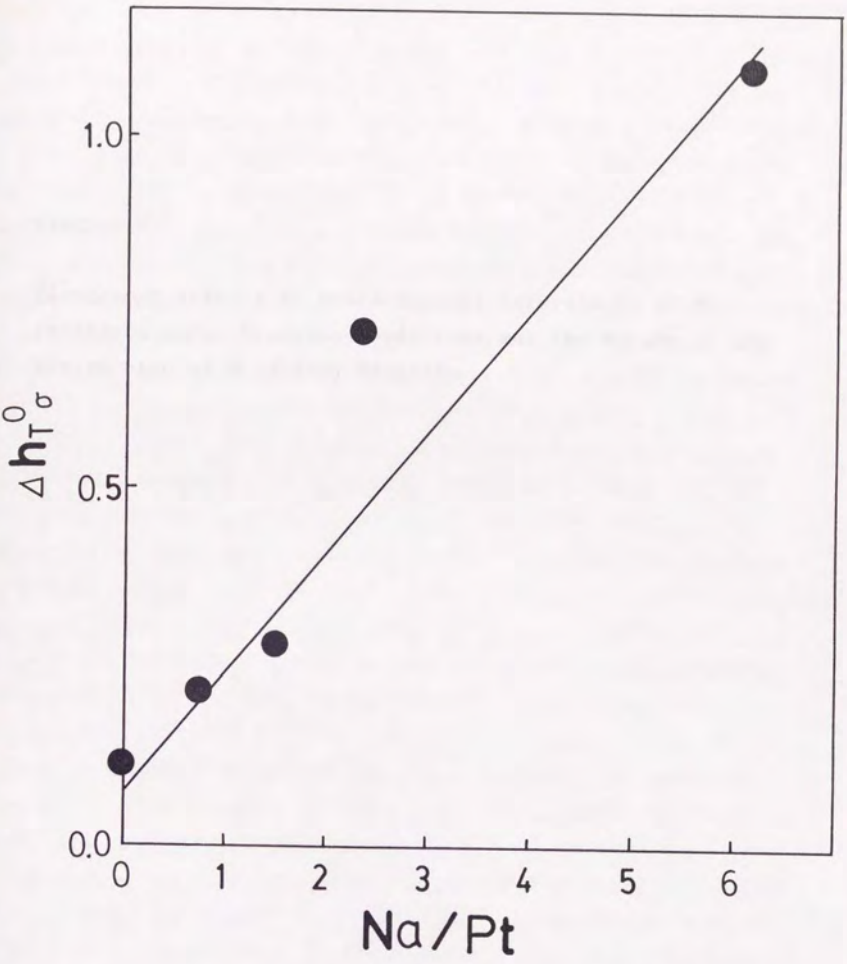

Figure 5.5 The number of electrons eliminated per an adsorbed di-σ-ethene ($\Delta h_{T}{}^{e}{}_{\sigma}$) as a function of Na loading.